14

Nanoparticles, Thin Films and Surface Patterns from Spin-Crossover Materials and Electrical Spin State Control

Paulo Nuno Martinho, Cyril Rajnak and Mario Ruben

Institute of Nanotechnology, Karlsruhe Institute of Technology

14.1 Introduction

Since the report of the first example of a spin-crossover (SCO) complex in 1931 by Cambi and co-workers[1] and the vision of Kahn and co-workers in 1996 towards the application of SCO compounds in data processing,[2] a long and impressive literature on SCO has developed with the discovery of several new examples of SCO compounds, the explanation of different types of SCO profiles, and the modification of SCO examples to increase cooperativity and to direct the application to materials science. Scientists have developed SCO networks,[3–5] SCO frameworks,[6–8] SCO gels,[9–11] SCO liquid crystals,[12–14] SCO nanoparticles and nanocrystals, SCO thin films and have also applied patterning techniques to fabricate SCO devices. More recently electrical control of SCO has been achieved and this work reviews research made so far with concern to nanoparticles, thin films, surface patterns and devices from SCO materials.

SCO complexes are a particular class of compounds of $3d^4$ to $3d^7$ transition metals ions in an octahedral (O_h) field, which can interchange between two electronic states, high spin (HS) and low spin (LS), by application of an external perturbation such as temperature, pressure, light or magnetic field.[15] This property can be either present in solution or solid state and while in solution the system is diluted and the process essentially molecular, in solid state the process may involve elastic interactions conferring different types and shapes of transition curves. SCO was first reported by Cambi and co-workers when they observed unusual magnetism in iron(III) derivatives of various dithiocarbamates which resulted in the recognition of the interconversion of two spin states as a result of variation in temperature.[1, 16, 17] Despite this discovery in the early 1930s a boom

Spin-Crossover Materials: Properties and Applications, First Edition. Edited by Malcolm A. Halcrow.

in SCO research has only occurred in the last 15 years with the miniaturisation of electronic devices and the approach of the superparamagnetic limit for magnetic materials.

14.2 Nanoparticles and Nanocrystals

A key factor in the application of SCO systems into materials development is the control of the size of the object that displays hysteresis.[18] For production of functional devices, the use of nanometre-range SCO materials is required and, combined with this, their magnetic and cooperative behaviour should be retained at low dimensions. SCO nanoparticles have been produced that mainly recur to two distinct families of compounds: the $[Fe(R\text{-}trz)_3]X_2$ family (trz = 1,2,4-triazole) and the $[Fe(pz)]\{M(CN)_4\}$ family (pz = pyrazole). The results obtained for SCO nanoparticles derived from $[Fe(R\text{-}trz)_3]X_2$ (Fig. 14.1) have been very interesting.

14.2.1 Reverse Micelle (Microemulsion) Technique

In this technique, the resultant particle volume is defined by the size of the water droplet within the emulsion. The most effective way to control the water droplet size is to vary the relative ratio of the water-to-oil, such that smaller droplets are formed when the amount of oil is increased.[19, 20]

Diverse techniques have been used to produce SCO nanoparticles but undoubtedly the most widely used has been the reverse micelle method, Fig. 14.1. This section reviews work done to produce SCO nanoparticles using reverse micelle, dispersion and sol-gel techniques.

14.2.1.1 Triazole Derivatives

Coronado pioneered the preparation of SCO nanoparticles using the reverse micelle type technique, which used either a water-in-oil or ethanol-in-oil microemulsion to grow SCO nanoparticles of $[Fe(Htrz)_2(trz)](BF_4)$ which were purple in colour and with an average size of around 15 nm.[21] Evaporation of the solvent produced a solid that could be suspended in *n*-octane yielding a bright transparent suspension. The thermochromic behaviour of such suspensions was investigated, with the nanoparticles presenting a colour change associated with both HS (pink) and LS (colourless) states. Transmission electron microscopy (TEM) images of isolated particles showed regular sized spherical nanoparticles, Fig. 14.2a. Magnetic investigation of the isolated

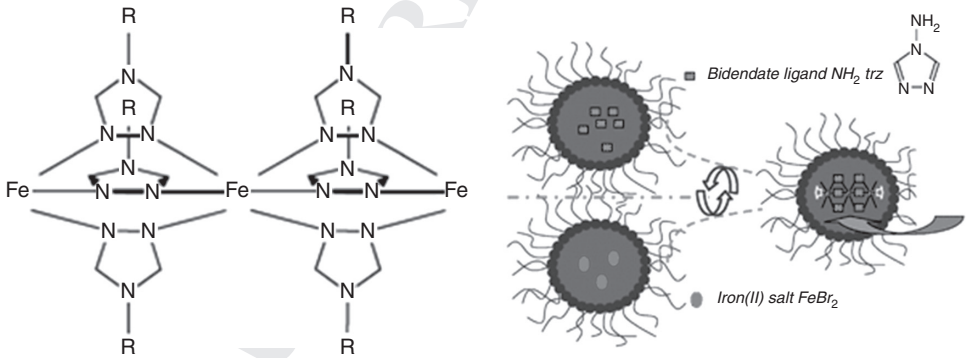

Figure 14.1 *Iron(II) triazole-nanoparticles. (Left) representation of main family of compounds ($[Fe(R\text{-}trz)_3]X_2$) used to produce SCO nanoparticles; (right) synthetic route used to produce nanoparticles of $[Fe(NH_2\text{-}trz)_3]$. Reproduced from ref. 22. Copyright Royal Society of Chemistry.*

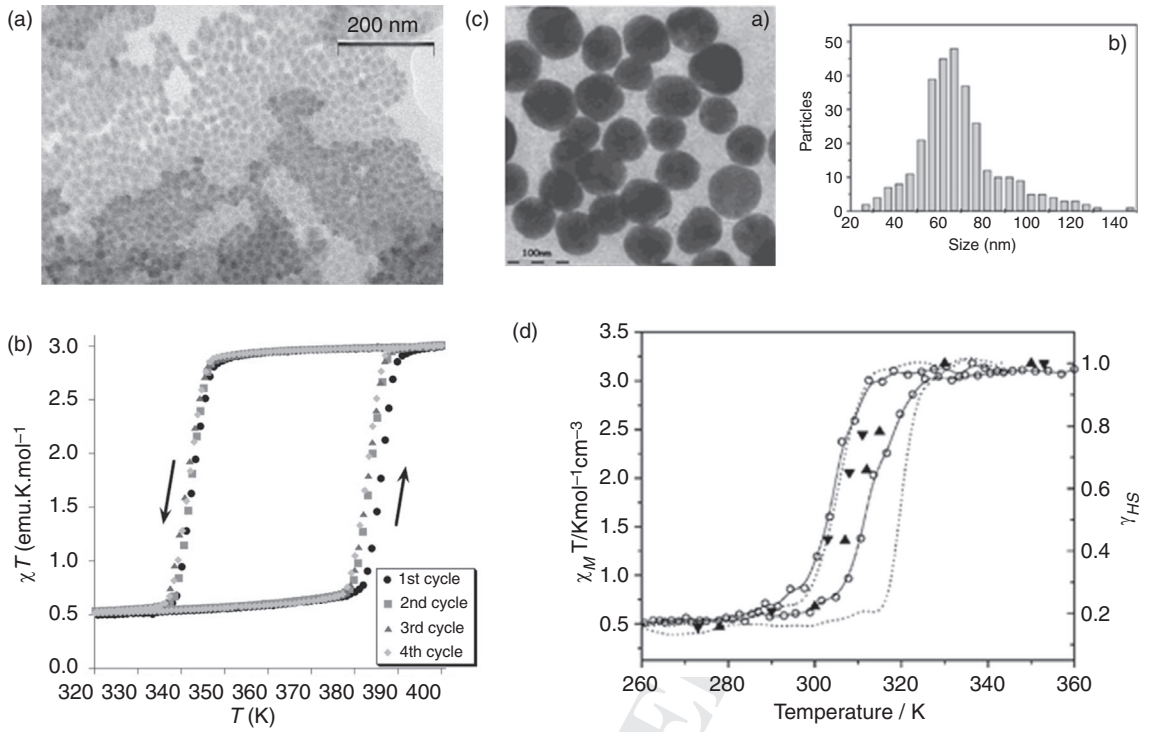

Figure 14.2 *SCO nanoparticles of ([Fe(R-trz)$_3$]X$_2$: (a) TEM image of [Fe(Htrz)$_2$(trz)](BF$_4$) nanoparticles; (b) magnetic thermal hysteresis of [Fe(Htrz)$_2$(trz)](BF$_4$) nanoparticles with 1st cycle represented by black circles, 2nd cycle represented by red squares, 3rd cycle represented by blue triangle and 4th cycle represented by yellow diamonds;[21] (c) TEM image of [Fe(NH$_2$trz)$_3$](Br)$_2$·3H$_2$O·0.03(surfactant) nanoparticles with statistic distribution based TEM images on ca. 300 particles, showing average size 69 nm, minimum and maximum sizes, 26 and 147 nm and disparity 19 nm; (d) Magnetic plot of [Fe(NH$_2$trz)$_3$](Br$_2$)·3H$_2$O·0.03(surfactant) for nanoparticles (-) and for macroscopic particles obtained from a typical synthesis (–). Reproduced from refs 21 and 22. Copyright Wiley VCH and the Royal Society of Chemistry.*

nanoparticles showed that both the transition temperature ($T_{1/2}\uparrow = 386$ K and $T_{1/2}\downarrow = 343$ K) and the large 43 K wide hysteresis window were preserved when compared to the original nonengineered powder samples, Fig. 14.2b.

In a parallel development Létard *et al.* prepared nanoparticles of a related compound where the triazole is appended with an amino function and the bromide salt is used, [Fe(NH$_2$-trz)$_3$](Br)$_2$·3H$_2$O.0.03(surfactant = Lauropal).[22] In contrast to the nanoparticles previously described, their hysteresis window is preserved only for large particles (>50 nm). It is interesting that these authors used a nonionic surfactant in contrast to sodium dioctyl sulfosuccinate used by Coronado and co-workers. TEM images of isolated nanoparticles dispersed in an ethanol solution, showed a good distribution of spherical particles with an average size of 69 nm, Fig. 14.2c.

Magnetic measurements for a collection of nanoparticles in both cooling and warming modes showed an 8 K wide hysteretic SCO system ($T_{1/2}\uparrow = 311$ K and $T_{1/2}\downarrow = 303$ K). When compared to the macroscopic particles (bulk sample) it was possible to observe that the width of the hysteresis window and consequently the degree of cooperativity decreases for the nanoparticles, Fig. 14.2d. In a follow up, Létard and co-workers applied the

same reverse micelle technique to the previously studied system and analysed the influence of the particle size on the SCO properties.[23] In a controlled fashion, particles with different sizes were produced by changing the surfactant/water ratio. TEM images of the particles as function of the surfactant/water percentage ranging from 50–85% were obtained, Fig. 14.3a. The authors concluded that homogeneity increases and particle size decreases with increasing proportions of surfactant, yielding 30 nm size nanoparticles when 85% of surfactant was used.

The magnetic properties in cooling and warming modes as a function of surfactant/water percentage were determined, Fig. 14.3b. The abruptness of the transition was quantified using a parameter introduced by the authors (ΔT_{80}), corresponding to the difference of temperature at which 80 and 20% of the iron(II) metal ions undergo spin-transition. Examination of the magnetic plots concluded that although the transition temperature is not strongly influenced by the size of the particles, the width of the hysteresis is strongly dependent on the size of the particles. The authors also pointed out that irrespective of the particle size the materials display a large absorption shoulder at around 520 nm, as a result of the *d–d* transition of the LS state ($^1A_{1g} \rightarrow {}^1T_{1g}$). The *d–d* transition of the HS state ($^5T_{2g} \rightarrow {}^5E_g$) is expected to be observed at lower energy at 830 nm.

Recently, Coronado and Galán-Mascarós have studied the effect of chemical and size tuning on the thermal hysteresis of bistable SCO nanoparticles. Nanoparticles of $[Fe(Htrz)_2(trz)](BF_4)$, $[Fe(Htrz)_{3-x}(NH_2trz)_x](ClO_4)_2$ and $[Fe_{0.8}Zn_{0.2}(Htrz)_2(trz)](BF_4)$ were prepared using the reverse micelle technique. The authors observed that mean size of the $[Fe(Htrz)_2(trz)](BF_4)$ nanoparticles can be tuned down to 6 nm in diameter, with a considerable homogeneity shown by the narrow size distribution. The abruptness of the SCO was not affected by tuning down the size of the nanoparticles, which maintained thermal hysteresis loop widths of 30–40 K. Doped nanoparticles, $[Fe(Htrz)_{3-x}(NH_2trz)_x](ClO_4)_2$ and $[Fe_{0.8}Zn_{0.2}(Htrz)_2(trz)](BF_4)$, presented sizes ranging from 10–15 nm with SCO temperatures closer to room temperature and thermal hysteresis loops narrower than the ones produced by undoped nanoparticles (15–20 K). TEM, Fig. 14.4a–c, and atomic force microscopy (AFM), Fig. 14.4d and Fig.14.4e, after deposition on gold or silicon surfaces were used to characterise produced nanoparticles.[24]

Bousseksou *et al.* also contributed considerably to advance the research on SCO nanoparticles by preparing nanoparticles of $[Fe(NH_2trz)_3](tos)_2$ (tos = tosylate) doped with fluorescent Rhodamine 110 (Rh110), Fig. 14.5.[25] The authors choose Rh110 as fluorescent marker because this exhibits only a very weak thermal extinction of its luminescence around room temperature. Its emission spectrum and the low energy tail of its excitation spectrum both overlap the $^1A_{1g} \rightarrow {}^1T_{1g}$ absorption band of the iron(II)-triazole complex. Finally, Rh110 also exhibits relatively weak photobleaching, and its properties within reverse micelles had been previously explored by others.[26]

Undoped nanoparticles showed reversible thermochromic behaviour, with a violet suspension turning colourless when heated to 50 °C which indicated possible SCO behaviour, Fig. 14.5a. Fluorescence of 10(6) nm nanoparticles of $[Fe(NH_2trz)_3](tos)_2$ doped with 3% Rh110, and 3 nm nanoparticles of $[Fe(NH_2trz)_3](NO_3)_2$ doped with 0.01% Rh110, were investigated. The thermal variation of the fluorescence intensity at 540 nm showed that for $[Fe(NH_2trz)_3](tos)_2$ doped with 3% of Rh110, the transition temperatures are 301 and 306 K in the heating and cooling modes, respectively. In contrast to what would be expected, the authors observed that the emission intensity increases with the temperature. In the case of $[Fe(NH_2trz)_3](NO_3)_2$ nanoparticles doped with 0.01% of Rh110, the absence of hysteresis allowed the authors to develop a thermometer for real-time thermometry, Fig. 14.5c.

In parallel to the developments on fluorescent SCO nanoparticles, Bousseksou and co-workers also investigated the cooperative SCO phenomena in $[Fe(NH_2trz)_3](tos)_2$ nanoparticles.[27] Particles with 3–4 nm size were obtained using a nonionic surfactant to avoid anion exchange. TEM, high-resolution transmission electron microscopy (HRTEM), dynamic light scattering (DLS), UV-vis spectroscopy and magnetic measurements were used to characterise dried particles and particles in suspension. TEM images of nanoparticles of $[Fe(NH_2trz)_3](tos)_2$ show similar, spherical, nonaggregated nanoparticles with a narrow size distribution.

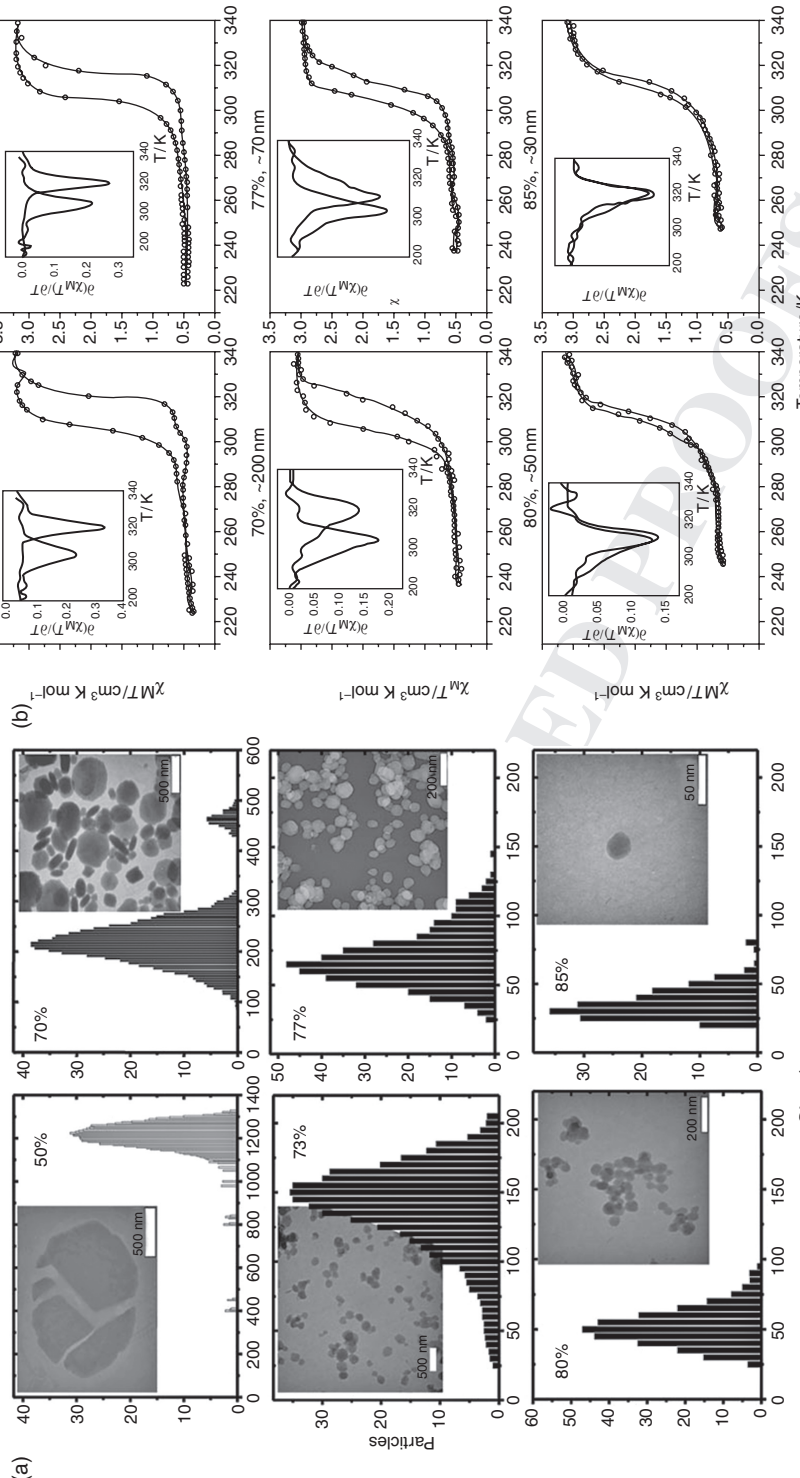

Figure 14.3 *Size distribution of $[Fe(NH_2trz)_3]Br_2$ nanoparticles: (a) Number of particles versus particle sizes from TEM images of nanoparticles prepared by a reverse micelle method as function of the surfactant/water percentage. Statistic distribution evaluated according TEM images on around 300 particles; (b) magnetic plots of $[Fe(NH_2trz)_3]Br_2{\cdot}y$(surfactant) for the macroscopic particles prepared on traditional way and for nanoparticles depending of the surfactant/water ratio. Reproduced from ref. 23. Copyright Wiley/VCH.*

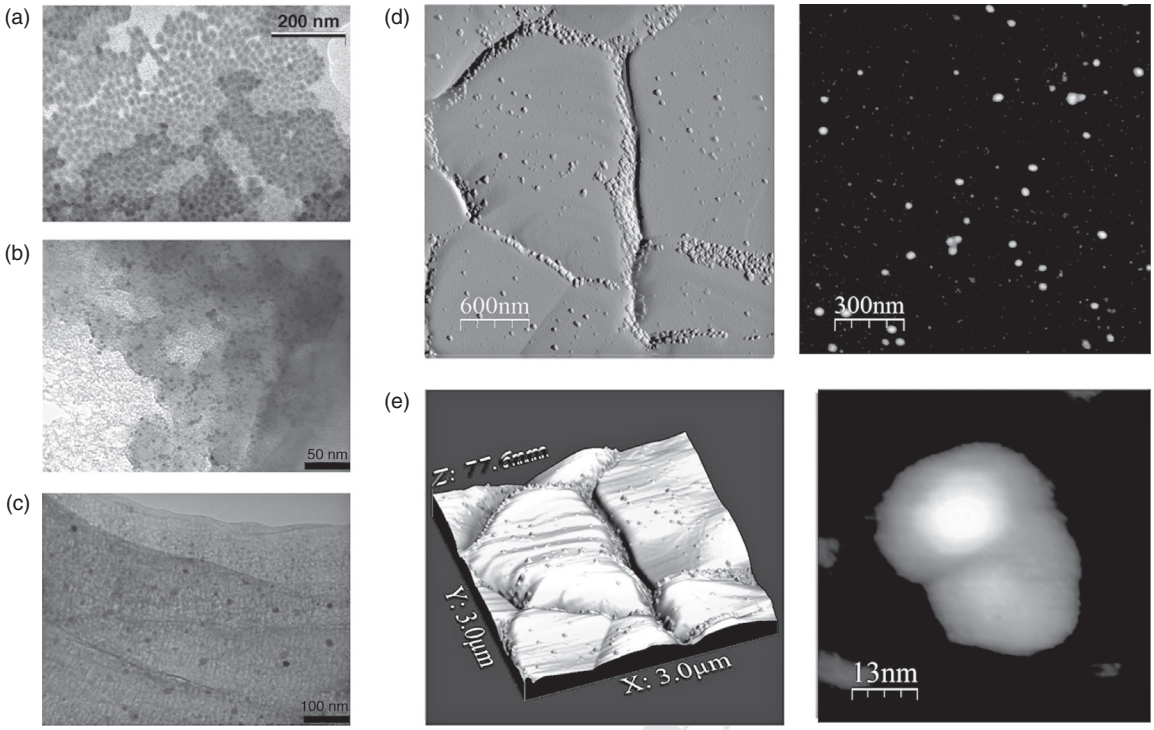

Figure 14.4 *Structural characterisation of SCO nanoparticles: (a) TEM image of NPs of [Fe(Htrz)$_2$(trz)](BF$_4$); (b) TEM image of NPs of [Fe(Htrz)$_{3-x}$(NH$_2$trz)$_x$](ClO$_4$)$_2$; (c) TEM image of NPs of [Fe$_{0.8}$Zn$_{0.2}$(Htrz)$_2$(trz)](BF$_4$); (d) AFM images of nanoparticles of [Fe(Htrz)$_2$(trz)](BF$_4$) on a gold substrate (left) and on a silicon substrate (right); (e) AFM high resolution topography image of nanoparticles of [Fe(Htrz)$_2$(trz)](BF$_4$) on a gold substrate. Reproduced from ref. 24. Copyright American Chemical Society.*

This was further confirmed by DLS at room temperature. The SCO behaviour of such particles was investigated by variable temperature UV-vis experiments by following the change in intensity of the LS absorption peak centred at 540 nm. Thermal SCO curves of [Fe(NH$_2$trz)$_3$](tos)$_2$ nanoparticles exhibit a sharp transition around $T_{1/2} = 295$ K, which was also confirmed by magnetic measurements on colloidal suspensions of the same sample. The authors also pointed out that heating the sample above 313 K changes the SCO properties of the [Fe(NH$_2$trz)$_3$](tos)$_2$ nanoparticles.

Colacio and Herrera applied the same principle to prepare and design bifunctional hybrid SCO silica nanoparticles, Fig. 14.6a.[28] The authors stated that silica is a particularly suitable material for the preparation of SCO silica nanoparticles systems because its high porosity allows for the incorporation of SCO compounds. Moreover, as silica does not absorb light and does not interfere with magnetic fields the SCO compounds inside the silica nanoparticles will keep their original optical and magnetic properties. $\{[Fe(Htrz)_2(trz)](BF_4)\}_n$ and doped $\{[Fe_{1-x}Zn_x(HTrz)_2(Trz)](BF_4)\}_n$ were used to produce three hybrids based on the ratio of Fe/Zn used. The resultant nanoparticles were characterised by TEM and high-angle annular dark-field-scanning transmission electron microscopy (HAADF-STEM) and their composition analysed by energy dispersive X-ray spectroscopy (EDX), Fig. 14.6b. The isolated SCO silica nanoparticles were finally functionalised by grafting the organic fluorophore 3-(dansylamido)propyltrimethoxysilane (dansyl) to the silica nanoparticles surface.

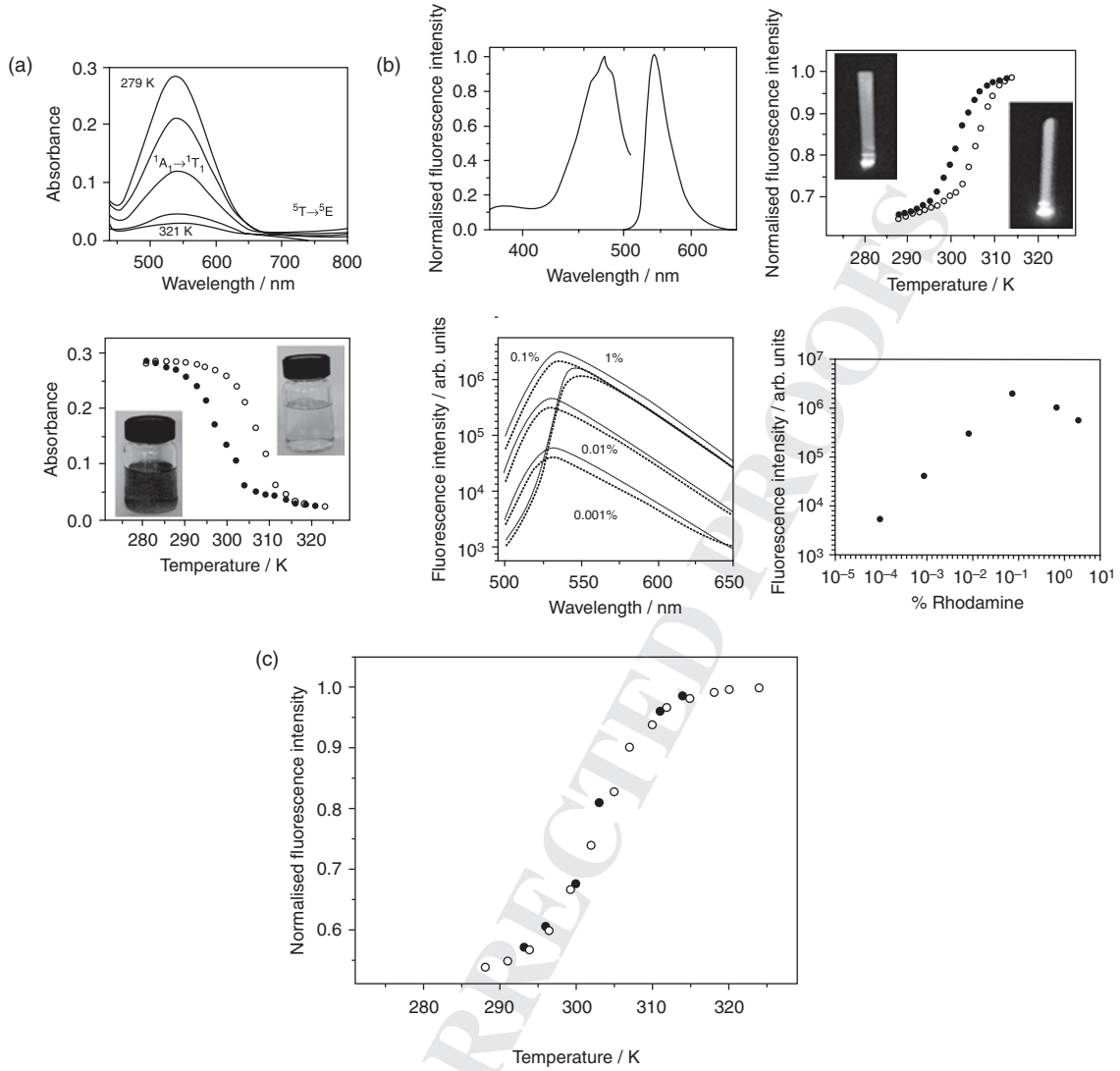

Figure 14.5 *Optical properties of $Fe(NH_2trz)_3(tos)_2$ nanoparticle suspensions: (a) (top) absorption spectra of an octane suspension of $Fe(NH_2trz)_3(tos)_2$ nanoparticles at selected temperatures in the cooling mode; (bottom) thermal variation of the absorbance of the suspension at 540 nm in the heating (open symbols) and cooling (closed symbols) modes, showing photographs of the sample at 295 K (violet) and 320 K (transparent); (b) (top-left) fluorescence excitation ($\lambda_{emission}$ = 540 nm) and emission ($\lambda_{excitation}$ = 475 nm) spectra of a rhodamine-110 doped (3%) $Fe(NH_2trz)_3(tos)_2$ nanoparticle suspension at room temperature; (top-right) thermal variation of the emission intensity at 540 nm in the heating (open symbols) and cooling (closed symbols) modes, showing photographs of a sample (0.001%) under white light excitation at 295 K and 320 K; (bottom-left) emission spectra of suspensions with diverse rhodamine concentrations. For each concentration the spectra were recorded successively at 288 K (solid line), 318 K (dashed line) and 288 K (dotted line); (bottom-right) fluorescence intensity maxima as a function of the rhodamine concentration (288 K); (c) thermal variation of the fluorescence intensity at 540 nm in the heating (open symbols) and cooling (closed symbols) modes for a 3 nm rhodamine-110 doped (0.01%) $[Fe(NH_2trz)_3](NO_3)_2$ nanoparticle suspension. Reproduced from ref. 25. Copyright Royal Society of Chemistry.*

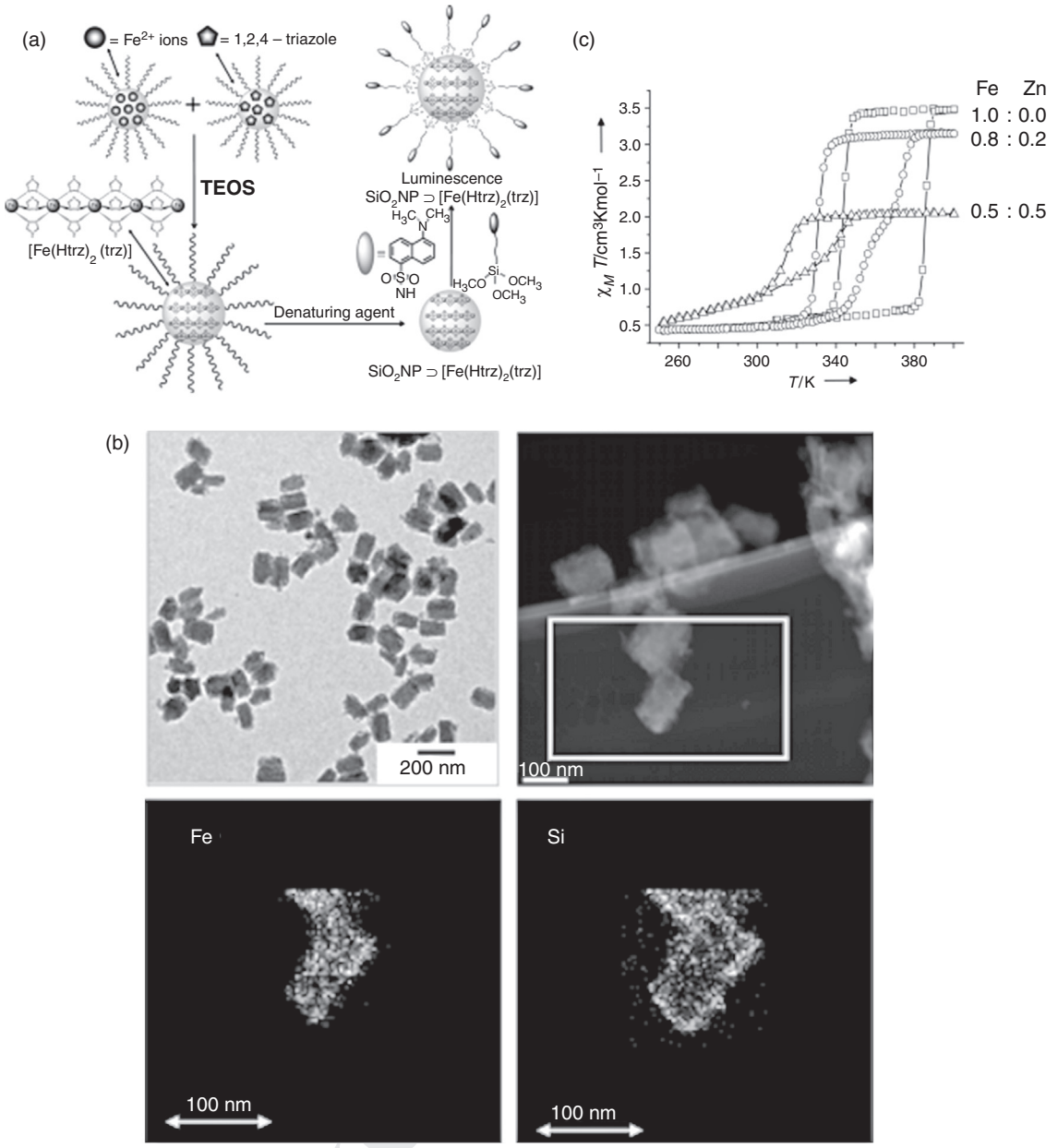

Figure 14.6 *SCO luminescent SiO_2 nanoparticles: (a) synthetic route; (b) TEM (top left) and high angle annular dark field-scanning transmission electron microscopy (HAADF-STEM) (top right) images of nanostructures of $\{[Fe_{1-x}Zn_x(HTrz)_2(Trz)](BF_4)\}_n$. EDX compositional maps of Fe (bottom left) and Si (bottom right) collected from the square area indicated on the HAADF-STEM image; (c) magnetic plots for different Fe/Zn ratios. Reproduced from ref. 28. Copyright Wiley/VCH.*

The size of the particles produced depends on the ratio of Fe/Zn used with average dimensions ranging from side length and width of 147 ± 11.7 nm and 92.1 ± 12.1 nm when no Zn is used to 188.9 ± 37.4 nm length and 28.8 ± 7.1 nm width when the ratio of Fe/Zn is 0.5:0.5. Silica nanoparticles grafted with dansyl have shown no significant difference in dimension when compared to the ungrafted nanoparticles.

Magnetic measurements on the three different silica nanoparticles showed that SCO behaviour is not lost when these are incorporated in silica or even when the system is diluted with Zn, Fig. 14.6c. For the undoped system, a complete and abrupt SCO was observed with $T_{1/2}\downarrow = 345$ K and $T_{1/2}\uparrow = 385$ K and a hysteresis loop of 40 K, which resembles the magnetic profile of the bulk sample.[29] For silica nanoparticles doped with Fe/Zn 0.8:0.2, SCO becomes less abrupt and shifts to lower temperatures with $T_{1/2}\downarrow = 330$ K and, in the warming mode, a stepped transition with $T_{1/2}\uparrow = 353$ K and $T_{1/2}\uparrow = 374$ K. Finally, for the system doped with Fe/Zn 0.5:0.5, the transition becomes rather smooth with $T_{1/2}\downarrow = 316$ K and $T_{1/2}\uparrow = 342$ K. Grafting the surface of SCO silica nanoparticles did not alter the magnetic profile of the nanoparticles. The authors also observed that the luminescence properties of the fluorophores grafted on the surface of the SCO silica nanoparticles can be adjusted by the spin state of the SCO polymer.

A very interesting approach has been described by Pillet and co-workers, who recently reported the preparation of nanoparticles of $[Fe(Htrz)_2(trz)](BF_4)$ using the reverse micelle technique and reverse hexagonal liquid crystalline phases.[30] The latter permitted the fabrication of polydispersive 1D nanoparticles which were characterised by variable temperature Raman spectroscopy. 1D nanoparticles have been shown to retain their SCO behaviour displaying abrupt SCO above room temperature with a hysteresis loop of 27 K.

14.2.1.2 Hofmann-Like Derivatives

SCO nanoparticles produced from Hofmann-like frameworks have also been prepared, Fig. 14.7a.[31] Catala and Mallah also used the reverse micelle technique which consisted of mixing a reverse microemulsion of $Fe(BF_4)_2{\cdot}6H_2O$ and pyrazine with a second microemulsion containing $K_2Pt(CN)_4$. This was followed by precipitation with *p*-nitrobenzylpyridine in the presence of the surfactant sodium bis(2-ethylhexyl sulfosuccinate). HAADF-STEM showed that the size of the particles is dependent on the concentration of metal ions used with sizes varying from 7.7 nm for higher concentrations to 40 nm for lower concentrations of metal ions, Fig. 14.7b. In the case of nanoparticles of Hofmann-like frameworks the SCO profile of the nanoparticles differs from the bulk powder, occurring at a lower temperature for the nanoparticle samples, Fig. 14.7c.

Matrix-dependent cooperativity in anisotropic SCO nanoparticles of $Fe(pyrazine)Pt(CN)_4$ was investigated by Catala and Mallah.[32] The authors tried to prove that the environment of the nanoparticles plays a crucial role in the SCO process and that the cooperativity can be tuned by the matrix surrounding the nanoparticles. TEM images showed mainly square-like particles with 10 × 10 nm. Matrix effects on the SCO and cooperativity of the system have been studied using two coating agents: a calixarene based ligand bearing 8 pyridine functions; and an inorganic polymer silica with thin and thick SiO_2 shells. Magnetic studies have shown that for particles with a thin silica shell, a hysteresis loop of 15 K is observed with transition temperatures close to room temperature. For calix-covered nanoparticles, only a very small hysteresis loop of 2 K is observed and no hysteresis was shown for the diluted composites whether in silica or in PVP.

SCO nanoparticles and nanocrystals of a 2D coordination polymer derived from $[Fe(3\text{-}Fpy)_2M(CN)_4]$ (M = Ni, Pd, Pt and 3-Fpy = 3-fluoropyridine) have also been prepared using the coating polymer poly(vinylpyrrolidone) (PVP), which was added to an aqueous solution of the starting materials and subsequent mixtures of these.[33] The bulk material, nanoparticles and nanocrystals have very distinct magnetic profiles. Their SCO properties are drastically influenced by the dimensions of the crystal or the particle. Square-like nanocrystals of Ni, Pt, and Pd derivatives with dimensions 400 × 400 × 30 nm, undergo a first order spin-transition. Earlier, other techniques, such as a variation of the reverse micelle synthesis, have been

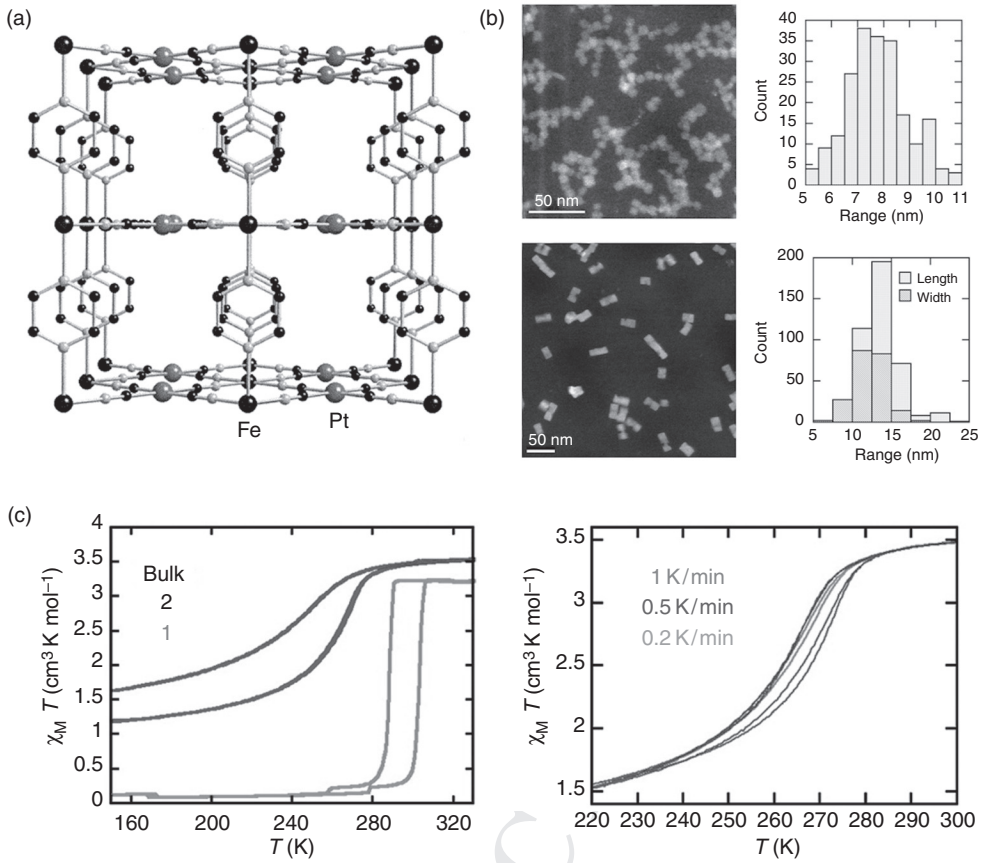

Figure 14.7 *SCO nanostructures derived from Hoffmann-like objects: (a) representation of a 3D network of Fe(pyrazine){Pt(CN)$_4$};[8] (b) HAADF-STEM imaging and size distribution of particles (top, scale-bar 50 nm and bottom, scale-bar 50 nm); (c) magnetic plots of the objects obtained from two different concentrations:* ***1****, 0.14 mol L^{-1} and* ***2****, 0.08 mol L^{-1} and bulk compound at a sweep rate of 1 K min^{-1} (left) and for 0.08 mol L^{-1} at three different sweep rates (right). Reproduced from ref. 31. Copyright American Chemical Society.*

used to give surfactant-free nanocrystals of [Fe(pz)Pt(CN)$_4$] displaying size-dependent SCO with hysteresis.[34] Ultra-small monodisperse nanoparticles of the 3D SCO coordination polymer [Fe(pyrazine){Ni(CN)$_4$}] obtained using the biopolymer chitosan as matrix were also reported with these particles retaining the cooperative SCO behaviour.[35]

14.2.1.3 Pyridyl Derivatives

In 2010 Létard *et al*. investigated light-induced storage of information in nanoparticles.[20] Nanoparticles of [Fe(NCS)$_2$(bpe)$_2$] [bpe = 1,2-bis(4′-pyridyl)ethane] were prepared by the water-in-oil reverse micelle technique, varying the amount of surfactant used, Fig. 14.8a. The reactant concentration was kept constant (0.05 M) and the mass of the nonionic polyoxyethylenic surfactant Ifralan D0205 was varied between [Fe(NCS)$_2$(bpe)$_2$]-25%, [Fe(NCS)$_2$(bpe)$_2$]-78%, [Fe(NCS)$_2$(bpe)$_2$]-85%. The consequences of particle size reduction on light-induced and thermally induced SCO properties have been investigated. TEM images of

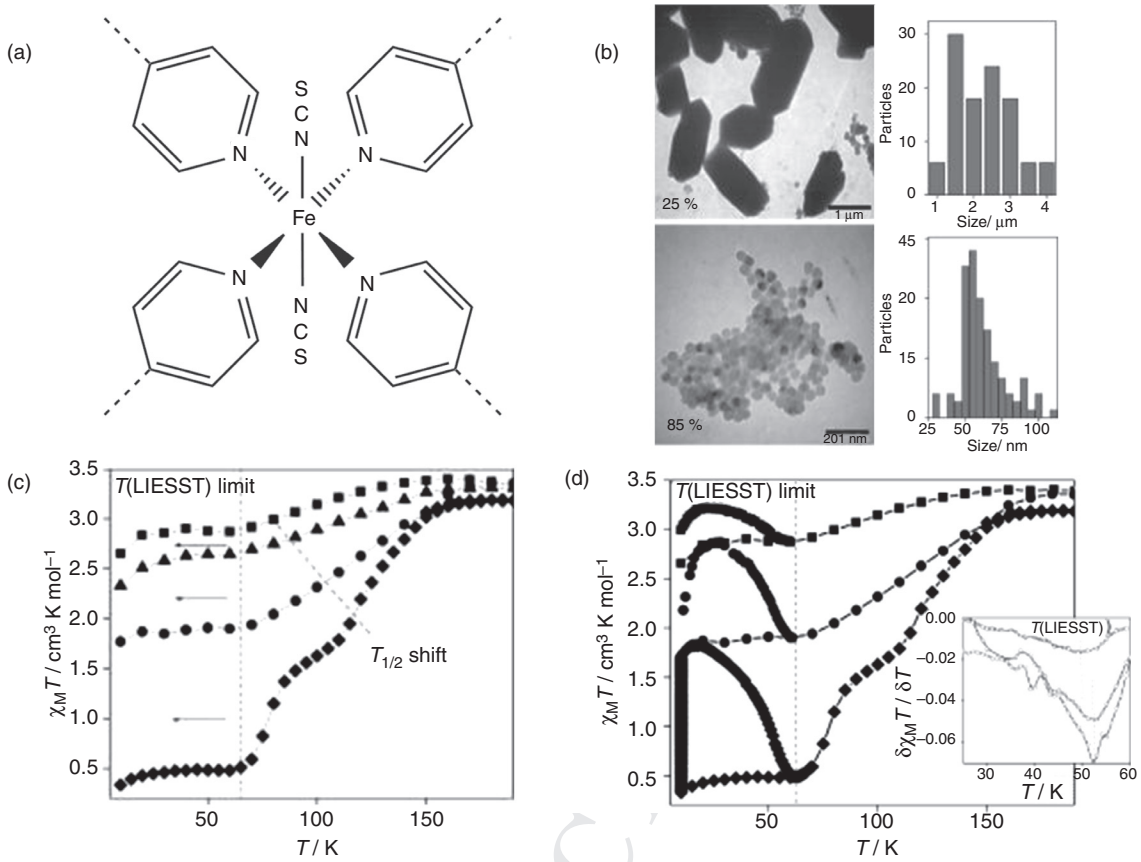

Figure 14.8 *Nanostructures from [Fe(NCS)$_2$(bpe)$_2$]: (a) structure of the compound used to produce nanoparticles; (b) (top) TEM images when 25% of surfactant was used (1–4 μm) and (bottom) when 85% of surfactant was used (30–80 nm) with respective size distribution histograms; (c) magnetic plot for bulk [Fe(NCS)2(bpe)$_2$] (♦, $T_{1/2}$ = 80/133 K), [Fe(NCS)$_2$(bpe)$_2$]-(25%-surfactant) (●, $T_{1/2}$ = 120 K), [Fe(NCS)$_2$(bpe)$_2$]-(78%-surfactant) (▲, $T_{1/2}$ = 110 K), [Fe(NCS)2(bpe)$_2$]-(85%-surfactant) (■, $T_{1/2}$ = 90 K); (d) magnetic plot for the thermally induced and light-induced SCO of bulk [Fe(NCS)$_2$(bpe)$_2$] (macroscale particles, ♦), [Fe(NCS)$_2$(bpe)$_2$]-(25%-surfactant) (microscale particles, ●) and [Fe(NCS)$_2$(bpe)2]-(85%-surfactant) (nanoscale particles, ■). Reproduced from ref. 20. Copyright Wiley/VCH.*

the particles showed that their size is dependent on the amount of surfactant used. This is not surprising, as it had been previously shown. For lower amounts of surfactant the particles show rod-like features with sizes ranging 1–4 μm. The size can be tuned down to 30–80 nm when 85% of surfactant is used, Fig. 14.8b.

Unlike the bulk material, the magnetic profile of the nanoparticles shows a slow one-step SCO for all amounts of surfactant used with $T_{1/2}$ shifting to lower temperatures with increasing of the amount of surfactant used, Fig. 14.8c.

Light-induced excited spin state trapping effect (LIESST) was investigated by sample irradiation at 10 K with light working at $\lambda = 530.2$ nm. A light-induced excitation of the LS state to a metastable HS state was observed with the degree of conversion being dependent of the amount of surfactant used and consequently the size of the particles, Fig. 14.8d.

14.2.2 Sol-Gel Techniques

Alternative techniques to the reverse micelle method to prepare nanoparticles have been used by Boillot and co-workers to give access to thermo and photoswitchable SCO nanoparticles of an Fe^{II} complex trapped in transparent silica thin films.[36] For that the authors used the sol-gel technique to fabricate nanoparticles of discrete molecules based on $[Fe((mepy)_3tren)](PF_6)_2$ ($(mepy)_3tren$ = tris(4-[(6-Me)-2-pyridyl]-3-aza-3-butenyl)amine), Fig. 14.9a. Nanoparticles were produced by mixing the crystalline solid in a previously aged solution containing tetramethoxysilane (TMOS), dimethyldimethoxysilane (DMDMS), acetone and H_2O.

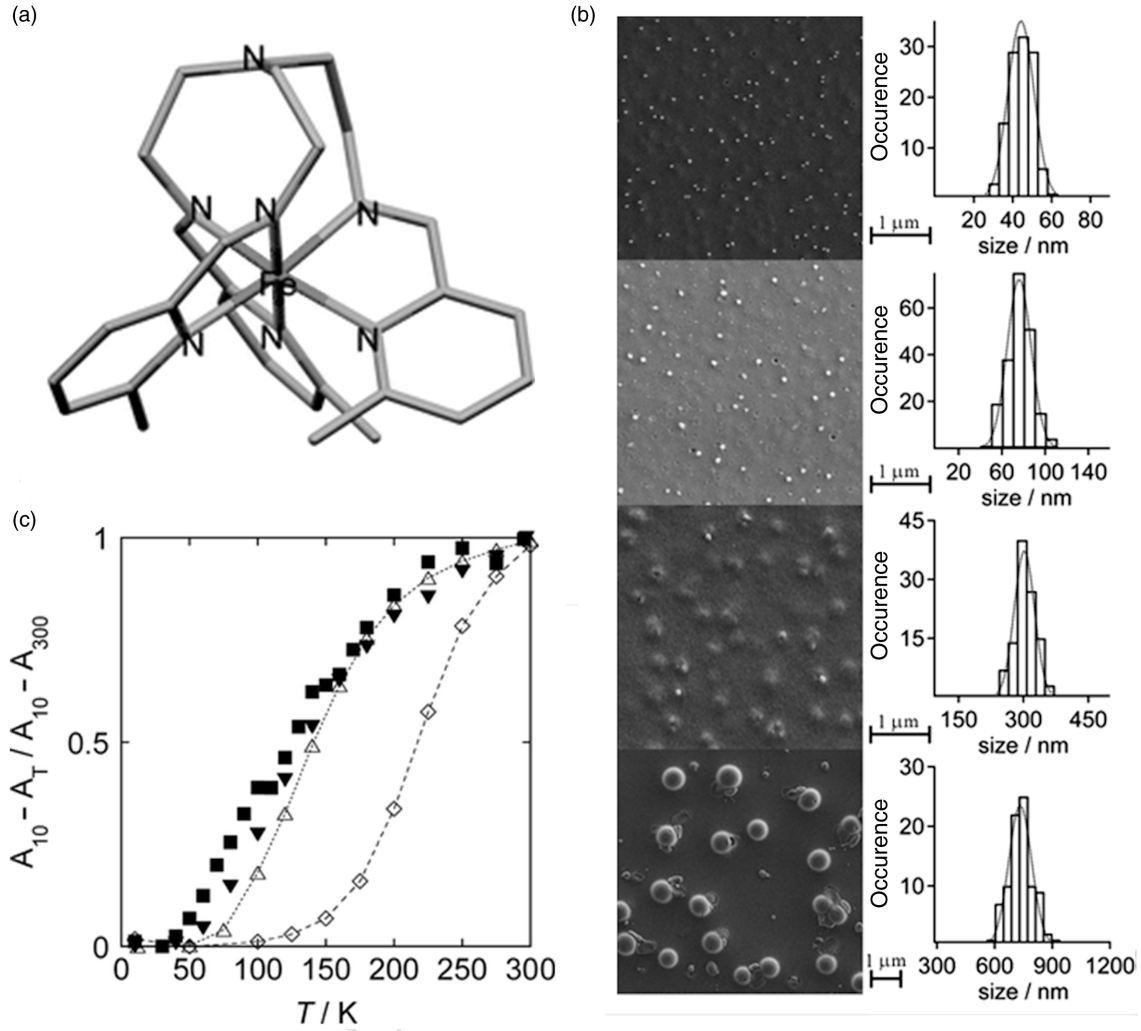

Figure 14.9 *Sol-gel technique to produce SCO nanoparticles: (a) molecular formula; (b) SEM images of $[Fe((mepy)_3tren)](PF_6)_2$ nanoparticles embedded in silica thin films; (c) relative area variation of MLCT absorption extracted from the Vis absorption data for 47 nm nanoparticles (▼), 730 nm nanoparticles (■), precipitated powder (Δ) and crystalline powder (◊). The ratio $(A_{10} - A_T)/(A_{10} - A_{300})$ corresponds to the fraction of SCO compounds in the HS state. Reproduced from ref. 36. Copyright Royal Society of Chemistry.*

The obtained solution was then spin-coated on a glass slide where rapid evaporation of solvents quenches the growth of the particles in the silica thin film. Nanoparticles with different dimensions were obtained depending on the aging time of the sol, giving particles with dimensions of 730 (± 80), 300 (± 40), 72 (± 16) to 47 (± 10) nm after 1 h, 2, 10 and 15 days, respectively, Fig. 14.9b.

Variable-temperature magnetic measurements were carried out both for the microcrystalline and the precipitated powders. Although the nanoparticles show thermochromic behaviour, magnetic measurements on thin films of nanoparticles prepared by spin coating were inconclusive and the authors used variable temperature UV-vis to probe the spin-transition in the nanoparticles, Fig. 14.9c. These have shown that the nanoparticles have a magnetic behaviour very similar to that of the precipitated powders with $T_{1/2} = 130 \pm 5$ K resulting in decreased cooperativity when compared to the crystalline sample. The authors also observed that the magnetic profile of the nanoparticles is size independent. Like the precipitated powders, the nanoparticles also show LIESST effect.

Faulmann *et al*. prepared nanoparticles of the SCO complex $[Fe(Htrz)_2(trz)](BF_4)$ in xerogel transparent composite films.[37] The dispersion and consecutive inclusion of the iron complex in a silica matrix prepared from TMOS or tetraethoxysilane (TEOS) afforded monoliths or films with a violet colour at room temperature, which turns white above 380 K. Particles with sizes ranging from 1 to 5 nm were imaged by TEM and their composition was confirm by EDX. Magnetic measurements showed that for films of nanoparticles in TMOS the transition temperatures shifted towards higher temperatures with the hysteresis loops also getting narrower with the number of cycles like the bulk sample. The SCO of crushed thin films and as prepared thin films was further confirmed by variable temperature Raman.

14.3 Thin Films

The engineering of SCO molecules towards processable memory devices is the main goal of applied SCO research. One of the most active routes pursued has been the deposition of such SCO active molecules on surfaces. For this, several techniques have been used (Langmuir–Blodgett (LB) deposition, surface-assisted molecular self-assembly, dip coating/drop casting, spin coating, complexes imbedded into matrixes), although only a few of these have been successful. One technique which has been most used to fabricate thin films of SCO active molecules is LB deposition. This and the other surface deposition techniques are reviewed below.

14.3.1 Langmuir–Blodgett Deposition

A single layer of molecules on a liquid–air interface is termed a *Langmuir monolayer*, and after transfer, is termed an *LB film*. It may be possible to transfer the monolayer to a surface if the surface substrate is immersed into and emmersed carefully from the trough. More than one layer may be transferred by successive immersions and emersions, although this is not always possible. Upon LB layer formation on a surface three different film architectures can result. Y-type multilayers are most common and X-type and Z-type films are rare.[38]

The first attempts to form a SCO LB film were made by Kahn and Ruaudel-Texier using an amphiphilic derivative of the well-known $[Fe(phen)_2(SCN)_2]$ complex, Fig. 14.10a.[39, 40]

The LB film of this complex was transferred onto calcium fluoride and quartz substrates accomplishing a successful transfer of up to 200 layers, Fig. 14.10b. The type of film was inconclusive and of type X or Z and has been shown by variable temperature IR to exhibit thermal SCO with $T_{1/2} = 260$ K and a hysteresis loop of ca. 4 K, Fig. 14.10c.[40]

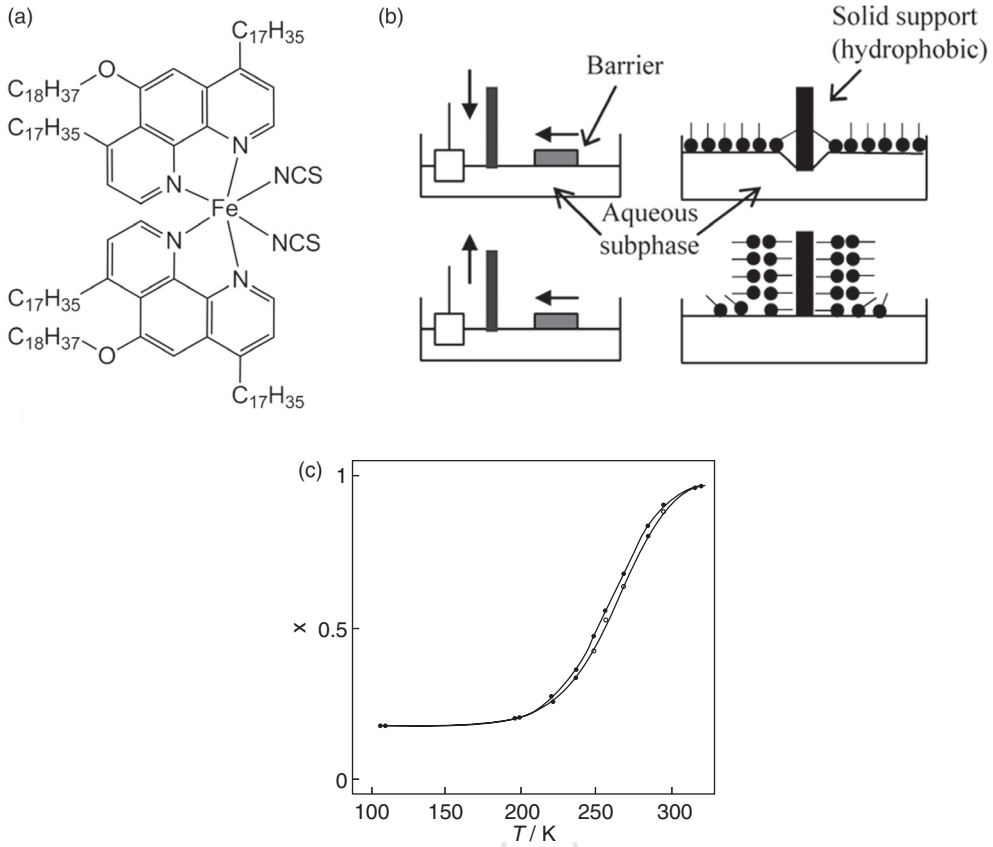

Figure 14.10 *Production of SCO LB films: (a) molecular structure of [Fe(phen)$_2$(SCN)$_2$] derivative;[39, 40] (b) Langmuir–Blodgett deposition on a surface starting with a hydrophobic substrate;[38] (c) temperature dependence of molar fraction of HS species in both cooling and warming modes based on vibrational modes changes followed by IR. Reproduced from refs 38 and 40. Copyright American Chemical Society and the Royal Society of Chemistry.*

Later in 1998, Mingotaud and co-workers studied the formation of Langmuir and LB films on a derivatised [Fe(bpy)$_2$(SCN)$_2$] with bpy = 2,2′-bipyridine. Langmuir films were found to be very unstable when formed at the air–water interface. The problem was overcome when a mixed liquid phase was used. The stability of the Langmuir films increased considerably when a water:DMF mixture was used as liquid phase, and a further increase in stability was achieved when a mixture of water:DMF:KNCS was used. Y-type LB multi-layered films were transferred onto a calcium fluoride substrate and characterised by variable temperature IR spectroscopy. The SCO showed a quite distinctive profile if the magnetic measurements on the film were performed below 340 K (gradual and incomplete with $T_{1/2} = 292 \pm 7$ K), or by heating above 340 K. The latter transition is more abrupt and complete than the former cycle, but is irreversible.[41, 42]

A third Fe(II) LB film was obtained using a small variation of the bpy ligand described in the previous example. Langmuir films obtained using an aqueous solution of KSCN as subphase and complexes with a ligand derived from bpy with R groups $(CH_2)_{12}$-$(CF_2)_5$-CH_3 and Me were transferred onto a Mylar substrate.

Multilayered (>1200 layers) LB films were also shown to display thermal SCO with hysteresis. Furthermore, the complex was shown to present the Light Induced Excited Spin State Trapping (LIESST) effect, showing a more efficient LIESST process when compared to the powdered sample.[43–45]

Armand *et al.* used the same approach to fabricate LB films of the alkylated coordination polymer $[Fe(C_{18}trz)_3]X_2$ (X = perchlorate, triflate, tosylate).[46] The attempts were not successful due to the instability of the complexes at the air–water interface.[46] This is not surprising, as LB films of SCO complexes have often exhibited assembly problems, due to chemical instability of the iron complexes at the air–water interface and consequent hydrolysis of the coordination bonds, or oxidation of the metal centres. Attempts to minimise the hydrolysis have included the use of a DMF-water mixture as the subphase instead of pure water, and the use of semifluorinated chains to avoid organic solvents. A very interesting approach by Roubeau towards stabilisation of the Langmuir films at the air–water interface was the use of aqueous solutions of metal salts as a subphase. Solutions of $Co(NO_3)_2$, $Ni(NO_3)_2$ and $Zn(NO_3)_2$ all proved successful. These salt solutions permitted closer packing and formation of stable Langmuir monolayers, which were suitable for the fabrication of up to 1100 LB multilayers.[47] When this technique was applied to SCO complexes, partial thermal SCO in $[Fe(C_{18}trz)_3](NO_3)_2$ polymers was detected by magnetic measurements of 400–1100 LB multilayers deposited from a subphase containing $Fe(NO_3)_2$. For subphases containing other metal salts, no SCO was observed in LB films of $[Fe(C_{18}trz)_3](NO_3)_2$ polymers.[47, 48]

A different and more recent approach was developed by Kurth and co-workers where they fabricated LB multilayers using a polyelectrolyte-amphiphile complex (PAC). PAC were formed by self-assembly of a metallo-supramolecular polyelectrolyte (MEPE) based on the ditopic bis-terpyridine 1,4-bis(2,2′:6′,2″-terpyridine-4′-yl)benzene and dihexadecyl phosphate (DHP). LB films of PAC with 11–15 layers have been prepared and structurally characterised.[49, 50] Unlike the bulk material, the SCO of the PAC LB films is incomplete but reversible.[51, 52]

Brooker and Albrecht have used the LB technique to prepare Langmuir films of discrete Fe(II) complexes which have been shown to be very unstable.[53] More recently they have shown that functionalisation of the 3,5-di(2-pyridyl)-4*H*-1,2,4-triazole (dpt) ligand with a C_{16} aliphatic chain forms a SCO Fe(II) complex, $[Fe(C_{16}dpt)_2(NCS)_2]$, with $T_{1/2}$ = 290 K. This Fe(II) complex was also found to form stable Langmuir monolayers at the air–water interface but no attempts to form LB films were reported.[54]

Recently Albrecht and Morgan extrapolated these same principles to Fe(III), Co(III) and Mn(III) amphiphiles. The authors reported the formation of stable Langmuir films with redox stable Fe(III) amphiphilic complexes derived from $[Fe(sal)_2trien]^+$ (sal = salicylaldehyde, trien = triethylenetetramine), Fig. 14.11.[55] Although these complexes do not show SCO in the solid state, the longer C_{18} complex shows an abrupt SCO in solution.[56] Complexes with alkyl chains with a length ranging from six to eighteen carbons were tested and their ability to form Langmuir films was investigated. The authors observed that only the longer C_{18} complexes formed suitable Langmuir films for surface transfer. The transfer process was limited to four layers and the spectroscopic characterisation was inconclusive with respect to occurrence of LB film SCO.

The extension of similar amphiphilic systems to Mn(III) was accomplished by functionalisation of a ligand know to promote SCO with Mn(III) ions.[57] It was observed that in these ions the SCO is sensitive to the length and position of the alkyl chains with all spin transitions gentle and incomplete. It was also observed that the complexes with longer alkyl chains (C_{12} and C_{18}) formed densely packed Langmuir monolayers with intermolecular contacts occurring at earlier stages of compression for the C_{18}-functionalised complexes. Stability tests using the C_{18}-functionalised complexes have shown that only the complex bearing *cisoid* alkyl chains were able to form reasonably stable Langmuir films over extended periods of time. Attempts to transfer Langmuir films were not successful resulting in only partial transfer due to significant desorption of the material during downstrokes.

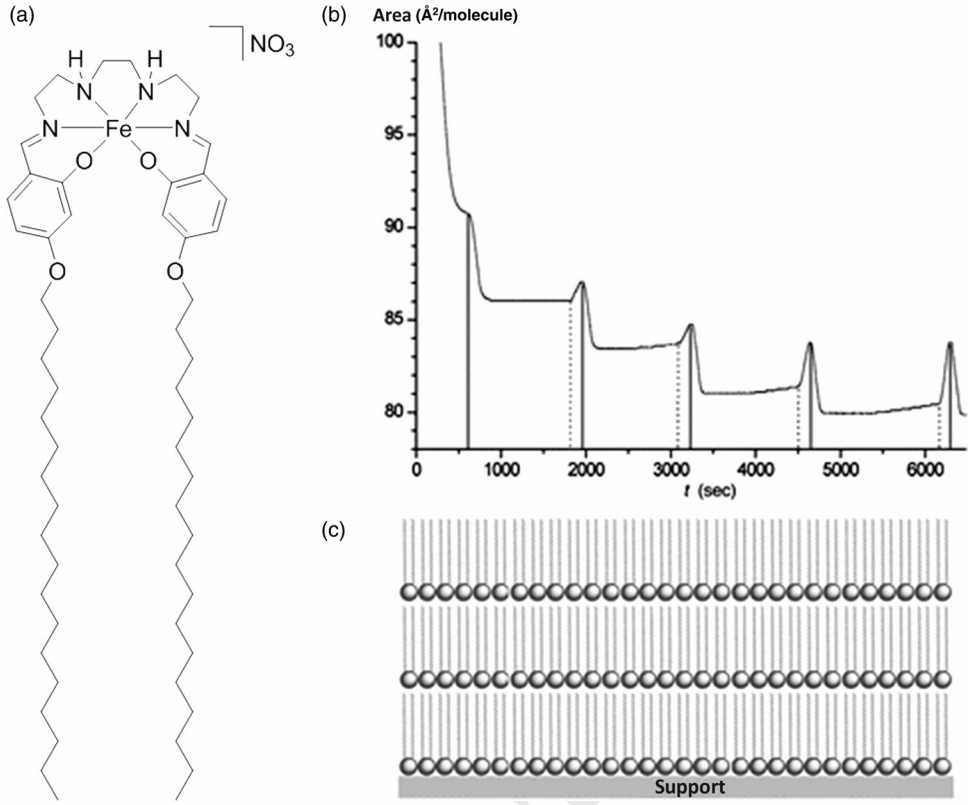

Figure 14.11 *Production of $[Fe(R\text{-}sal)_2trien]^+$ LB films: (a) C_{18} amphiphilic compound used to fabricate LB films; (b) Langmuir layers of $[Fe(C_{18}\text{-}sal)_2trien]NO_3$, transferred onto glass support; (c) representation of type of LB film formed. Reproduced from ref. 55. Copyright Royal Society of Chemistry.*

14.3.2 Surface-Assisted Molecular Self-assembly

A more successful approach than the LB technique is the multilayer sequential assembly (MSA) technique. This technique consists of the deposition/assembly of sequential layers by coordination bonds.[58, 59] Thus, Bousseksou and co-workers have prepared thin films with multilayers of the Hofmann-type SCO compound, $[Fe(pz)M(CN)_4]$ where M = Ni, Pd, or Pt using the MSA method by epitaxial growth on gold surfaces, Fig. 14.12a.[60]

The thin films formed by MSA retained the SCO characteristic of the bulk material. The SCO in the multilayers shows a 25 K wide hysteresis window centred around 310 K but the transition is less abrupt than in the powdered sample, Fig. 14.12b and 14.12c.

14.3.3 Diverse Techniques

Spin coating is a widely used and very versatile technique with several advantages. It is simple, cost effective, produces a low amount of waste, is rapid and highly reproducible and produces homogeneous films on a substrate. Spin coating is widely used in fabrication of inorganic nanostructure self-assemblies but major drawbacks are the limitation by the solvent and the lack of order after evaporation of the solvent.[61]

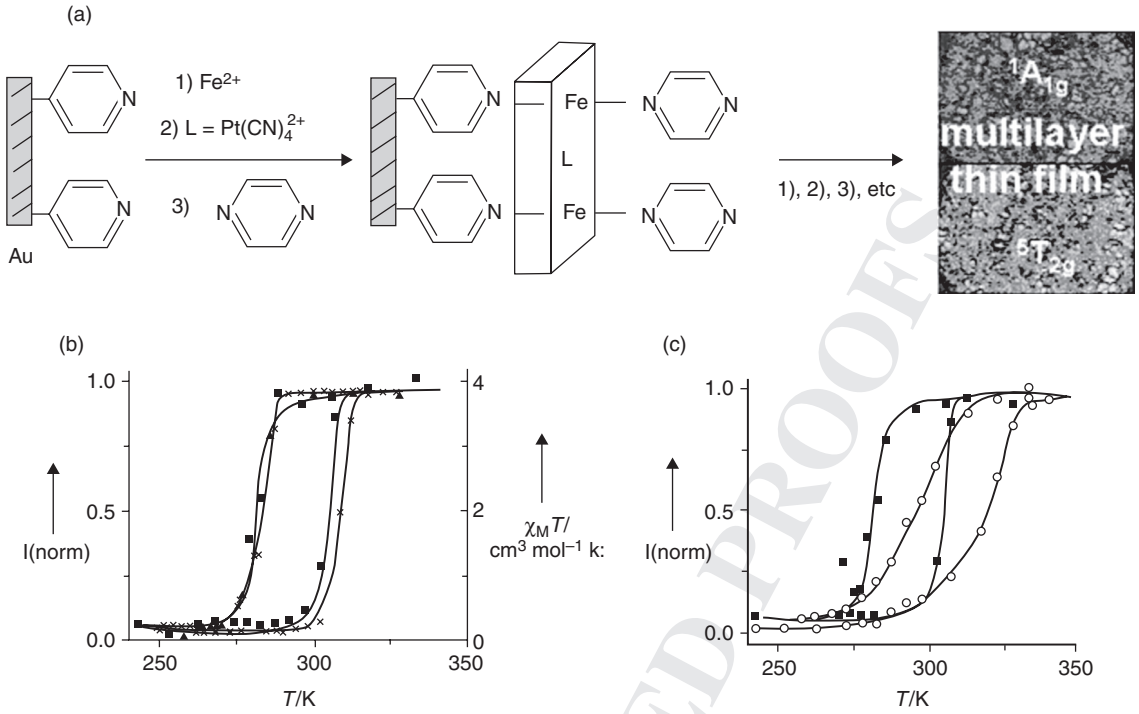

Figure 14.12 *Surface confined Hofmann-type SCO assemblies: (a) representation of SCO thin film formation of [Fe(pz)Pt(CN)$_4$].; (b) temperature dependence of the χ_mT product (×) and the normalised Raman intensity ratio (■) for [Fe(pyrazine)Pt(CN)$_4$] powder on cooling and heating modes. (c) Temperature dependence of the normalised Raman intensity ratio for [Fe(pyrazine)Pt(CN)$_4$] powder (■) and film (○) samples on cooling and heating modes. Reproduced from ref. 60. Copyright Wiley/VCH.*

The spin coating technique has also been applied to SCO complexes and the first report on attempts to fabricate a SCO thin-film by this technique was by Matsuda and Tajima.[62] $[Fe(dpp)_2](BF_4)_2$ (dpp = 2,6-di(pyrazolyl)pyridine) was chosen, which shows an abrupt spin-transition centred at 259 K with a 3 K hysteresis loop in the solid state, and a gradual transition in acetone solution. Smooth 30 nm thick films were prepared on a glass substrate from a saturated acetonitrile solution of the complex. The SCO property of the prepared film was investigated by variable temperature UV-vis spectroscopy and SQUID magnetometry and shows that these films show an abrupt and reversible SCO at ca. 260 K. Conductivity measurements performed on films sandwiched by indium-thin oxide (ITO) and aluminium over the SCO transition temperature have shown that there is a small change in resistivity with change in spin state.

As a follow up, the authors utilised the same SCO molecule and spin coating method to embed a SCO complex into a light-emitting layer of an EL device of chlorophyll *a*. By doping chlorophyll *a* with a SCO complex the authors achieved a drastic change of the EL intensity accompanying the SCO of $[Fe(dpp)_2](BF_4)_2$.[63]

A different approach has been developed by Kojima and co-workers, in which a Nafion film was doped with the SCO complex $[Fe(Htrz)_3]$.[64] The properties of thermal spin-transition as well as photoinduced SCO on the film have been reported. The Fe(II)-doped Nafion film was prepared by immersion of a Nafion film in an aqueous solution of an iron salt followed by immersion in a methanolic solution of 1,2,4-1H-triazole. The magnetic profile of the film, which shows a SCO around $T = 250$ K with a small hysteresis loop of about 5 K,

has been characterised in a separate report by Kojima *et al.* published around the same time.[65] Photoinduced SCO has been observed at low temperatures with an efficiency of conversion of 70% and decay dynamics suggesting that stochastic nucleation dominates the relaxation process. Later, the SCO behaviour of the film was further confirmed by Mößbauer spectroscopy.[66] The *P-T* phase diagram for the photoexcited steady state of the Nafion-[Fe(Htrz)$_3$] film has also been determined[67] and the same investigations have been extended to the parent system [Fe(NH$_2$-trz)$_3$]-Nafion. The prepared film shows a smoother SCO centred at 198 K.[68] To finalise the extensive work developed on these Nafion-[Fe(R-trz)$_3$] films, Kojima and co-workers reported in 2005 the preparation of transparent SCO Nafion-[Fe(Htrz)$_3$] film showing thermochromic behaviour changing from transparent (HS) to purple (LS).[69]

Recently, Kojima *et al.* demonstrated that the same principle can be applied to other SCO systems.[70] The elected candidate between the broad range of examples of Fe(II) SCO complexes has been [Fe^{II}(diAMsar)]$^{2+}$ (diAMsar = 1,8-diaminosarcophagine) where, as in the powdered samples, [Fe^{II}(diAMsar)]-Nafion films show a thermochromic dependence with the *p*H which is correlated with the SCO property of either the powder or the films.

Boillot reported poly(methyl methacrylate) (PMMA) polymeric films doped with the Fe(II) SCO complex [Fe(stpy)$_4$(NCSe)$_2$] (stpy = styrylpyridine).[71] Films were prepared from a mixture of PMMA with increasing amounts (2–20 wt %) of the [Fe(stpy)$_4$(NCSe)$_2$] complex. Transparent and semi-rigid PMMA doped thin films showed SCO at $T = 135 \pm 25$ K, which is comparable to that of the crystalline sample ($T_{1/2} = 163$ K).

Finally, vacuum deposition has been used to produce thin films of SCO complexes. This method can only be applied to molecules that are stable to decomposition under the ultra-high vacuum deposition conditions and has several advantages: it avoids dilution of the complexes embedded in a matrix; it allows exact control of the thickness of the films; and it can be applied to patterning techniques. Despite all these advantages, until now only two examples have been reported.

The first example was reported by Shi and Beaurepaire.[72] The authors described high-quality thin films of [Fe(phen)$_2$(SCN)$_2$] deposited on silicon or glass substrates by evaporation under high vacuum. However, the film morphology was shown to be sensitive to air and became coarse under ambient conditions. The composition of the film and confirmation of its integrity was demonstrated by X-ray photoelectron spectroscopy (XPS) on a 280 nm thick [Fe(phen)$_2$(SCN)$_2$] film. Optical transmission measurements were used to investigate the electronic structure of the films and the authors claimed that for films ranging from 7 to 530 nm the electronic structure of these remains practically unaltered. Moreover the magnetic profile of a 280 nm thick film was characterised by SQUID magnetometer measurements, showing that thicker films retain the SCO property with $T_{1/2} = 175$ K.

A more recent report by Quandt and Tuczek exploits the formation of thin films by high vacuum deposition method of SCO complexes exhibiting a LIESST effect.[73] The complexes studied were [Fe(H$_2$Bpz)$_2$(phen)] (H$_2$Bpz = bis(pyrazolyl)borate) and [Fe(H$_2$Bpz)$_2$(bipy)] (bipy = 2,2′-bipyridine). In the solid state, [Fe(H$_2$Bpz)$_2$(bipy)] shows a SCO centred at $T_{1/2} = 159.5$ K and a $T_{\mathrm{LIESST}} = 52$ K, while [Fe(H$_2$Bpz)$_2$(phen)] shows a SCO centred at $T_{1/2}\uparrow = 165.0$ K, $T_{1/2}\downarrow = 162.7$ K and a $T_{\mathrm{LIESST}} = 44$ K.[7] Thin films were deposited on ITO-coated glass or polymer tape and the thicknesses of the films were determined by a profilometer, their surface quality was investigated 4by AFM. A thin film of [Fe(H$_2$Bpz)$_2$(phen)] was prepared with a thickness of 480 nm and a rms roughness of 3.15 nm and a second thin film of [Fe(H$_2$Bpz)$_2$(bipy)] was also prepared with a thickness of 410 nm and rms roughness of 3.7 nm. The thermal and light-induced spin-transitions of the thin films were monitored by UV-vis absorption spectroscopy.

From the UV-vis spectra, the authors deduced the spin-transition temperatures for each of the thin films. For thin films of [Fe(H$_2$Bpz)$_2$(phen)] the $T_{1/2} = 155$ K ($\pm$ 1 K) which is comparable with the transition temperature of the solid sample ($T_{1/2}\uparrow = 165.0$ K, $T_{1/2}\downarrow = 162.7$ K). For thin films of [Fe(H$_2$Bpz)$_2$(bipy)] the $T_{1/2} = 166$ K ($\pm$ 1 K) which is also close to the transition temperature of the solid sample ($T_{1/2} = 159.5$ K).

LIESST-effect studies on thin films of both complexes were performed by irradiation of the film with a 525 nm wavelength light. For thin films of [Fe(H_2Bpz)$_2$(phen)], T_{LIESST} = 44 K with an efficiency of conversion to metastable HS of 83%. For films of [Fe(H_2Bpz)$_2$(bipy)], T_{LIESST} = 51 K with an efficiency of conversion to metastable HS of 85%.

14.4 Surface Patterns

The search for practical applications within the field of SCO either by insertion of active molecules into devices or by constructing devices out of SCO materials have brought together chemists and material scientists. In a different but complementary approach to those described above, Ruben and Cavallini, Molnár and Bousseksou, and finally Vieu, have investigated the possibility of depositing SCO compounds on surfaces through patterning techniques.

14.4.1 Surface Patterns of Spin-Crossover

Ruben *et al.* used discrete molecules to reproduce the pattern of a CD through lithographic techniques. For this the authors considered that the information generated in a SCO switching event occurs within the nanometric regime, thus the interfacing of the molecular switching units with the microscaled device environment would be of crucial importance. Considering this, the elected candidate for patterning was the neutral SCO complex *cis*-bis(thiocyanato)bis(1,10-phenanthroline)iron(II) which shows a thermal spin-transition centred at 176K, Fig. 14.13a.[75, 76]

The techniques used to deposit the SCO molecules on surfaces were Micro Injection Molding in Capillaries (MIMIC) to fabricate micrometric stripes and Lithographically Controlled Wetting (LCW) to pattern submicrometric and nanostructures, Fig. 14.13b. It has been observed that the SCO compound crystallises into micro- and nanowires or dots. Such patterns were characterised by AFM, polarised optical microscopy, grazing incidence X-ray diffraction (GIXD) and Raman spectroscopy.

AFM studies of structures of the SCO compound printed by MIMIC on silicon revealed the formation of strip-like structures (micrometric stripes) 1 μm in width, similar to the features of a stamp, Fig. 14.13c (left). Optical images obtained by polarised microscopy indicated behaviour typical for optically anisotropic materials exhibiting birefringence, Fig. 14.13c (centre and right). In particular, the microstripes appeared homogeneously coloured indicating that their thickness is almost constant over the entire stripe but changes between different stripes. Based on these observations it was deduced that confined deposition by MIMIC induced a coherent, long-range order along the length of the stripes. To obtain features in the nanometre regime the LCW technique was used. Structures with a resolution of approximately 160 nm were achieved, by estimation of the full width at half-maximum; below this limit the stamp features were not perfectly replicated.

The structure of nanopatterned films was investigated by GIXD. Azimuthal scans for both 010 and 001 reflections, forbidden for the original structure, were measured, indicating that the molecular arrangement (with loss of symmetry elements) is slightly different from that in the bulk, Fig. 14.13d. Finally, the authors aimed to pattern SCO representing information storage. For this, films of [Fe(phen)$_2$(SCN)$_2$] were moulded by LCW into a logic pattern replicating a recorded compact disk. The imaging of the patterned film by dark-field optical microscopy and AFM revealed an ordered array of crystallites of [Fe(phen)$_2$(SCN)$_2$]. The SCO was probed by variable temperature Raman performed on freshly prepared films, Fig. 14.13e. Freshly prepared films exhibited Raman spectra very similar to those of the powder retaining the SCO property.[75] This property was found to be unstable over time due to aging of the micro/nano architectures.

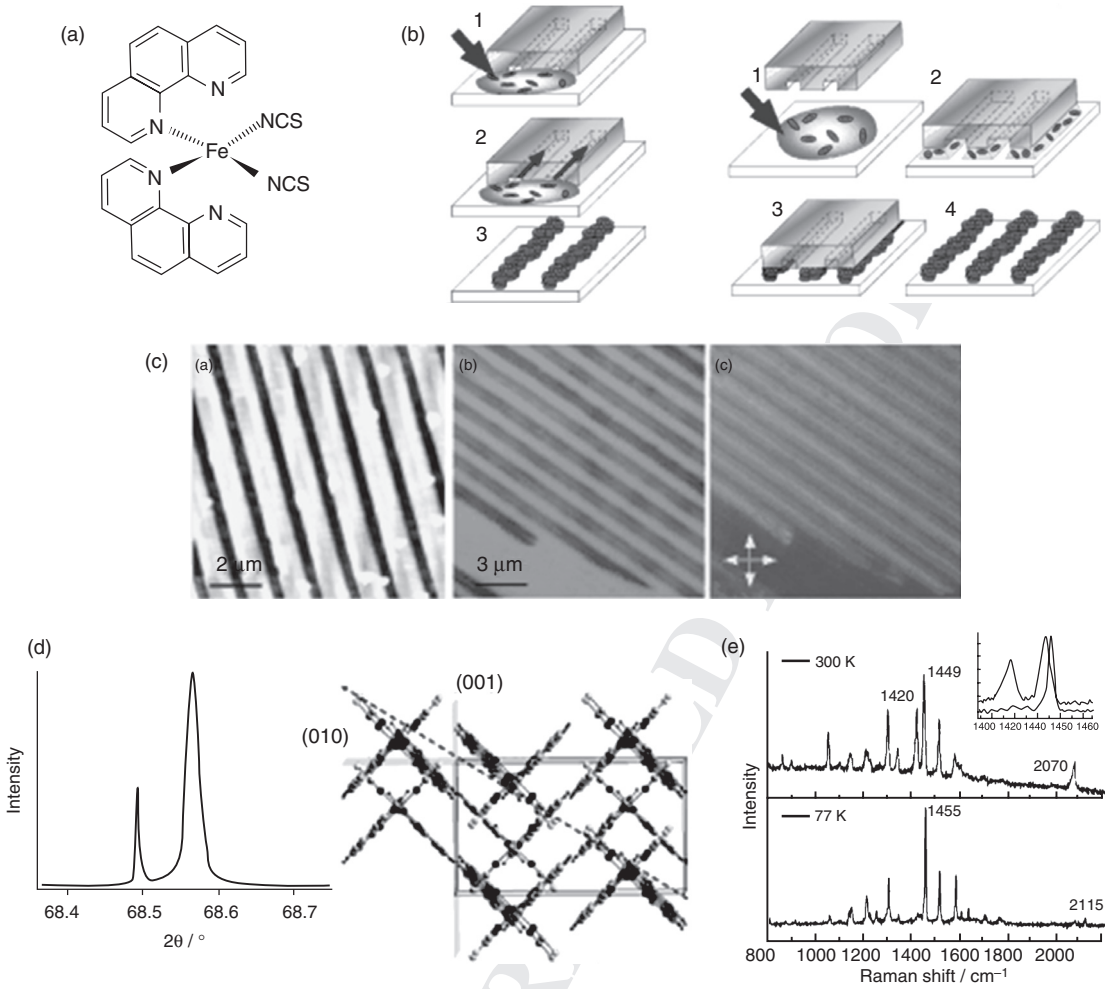

Figure 14.13 *Stamping of SCO nanostructures: (a) molecular structure of compound used to create patterns; (b) representations of the processes used to patterning SCO molecules; (c) microstripes of [Fe(phen)$_2$(SCN)$_2$] fabricated by MIMIC on a silicon surface: (left) AFM topography (z scale is 50 nm), (middle) optical micrographs recorded with unpolarised light, (right) micrographs recorded with crossed polars oriented along the axes of the image; (d) GIXD azimuthal scan for the (010) of microstripes printed by MIMIC and respective top view of the 3D structure of [Fe(phen)$_2$(SCN)$_2$] in the microstripes, as oriented in one domain. The red arrow indicates the orientation of the microstripes; (e) Raman spectra of freshly prepared films, at 300 and 77 K with SCO evident from the vibrational modes at 1449, 1420 and 2070 cm^{-1}. Reproduced from refs 75 and 76. Copyright Wiley/VCH and the American Chemical Society.*

More recently, the same authors built on the experience obtained with the previous system, to fabricate thin deposits and patterns of a room-temperature-switchable 1D SCO compound which crystallises to form an infinite 1-D chain exhibiting a SCO at $T = 286$ K.[77] With the aim of controlling the spatial distribution and the morphology of thin deposits, the authors used the LCW technique. The thin films and patterns prepared were characterised by AFM, polarised optical microscopy, XRD and Raman spectroscopy. Patterns of the

SCO compound prepared by LCW revealed the formation of stripe-like structures of 1 μm width, observed by optical microscopy and AFM.

It was found after a detailed AFM analysis of the morphology of the stripes, that the patterns show that each stripe is formed by rod-like crystallites. The SCO properties of these stripes were investigated by Raman spectroscopy. Raman experiments showed that the compound retains its SCO nature when the solvent shrinks slowly; interestingly, when fast shrinkage was employed, the thin deposit lost the ability to undergo SCO.

In 2007, Bousseksou and Molnár reported on a process for nano and microscale assembly of the 3-D SCO coordination polymer Fe(pyrazine)[$Pt(CN)_4$] which displays a very strong cooperative spin-transition with a ca. 25 K wide hysteresis loop centred around room-temperature.[78] These nano and microscale assemblies were produced using a combination of top-down (lift-off) and bottom-up (MSA) methods, employing a gold-coated silicon surface covered by a conventional polymethylmethacrylate (PMMA) EBL resist. Square-shaped patterns of different sizes and densities were written by a focused electron beam. After resist development, the substrates were dipped into a solution of 4,4′-azopyridine to prepare an anchoring layer for the thin film. Patterns of sizes ranging from 50 nm to 2 μm were created and imaged by SEM.

Limiting factors present during the process were desorption and re-adsorption accompanied by the formation of crystallites which originated 3-D crystallites with substantial roughness at large thickness. To probe the spin state of the micro and nanopatterned assemblies, Raman spectroscopy was used on patterns of 2 μm, 500 nm and 200 nm. Raman spectra of the larger nanopatterns allowed the identification of a thermal spin-transition where the vibrational mode at 1232 cm^{-1} changes dramatically in relative intensity. For smaller sizes the identification of the change in relative intensities was much more difficult, with arrays of 200 nm nanopatterns giving Raman spectra at both temperatures that were very similar, but sufficient for the authors to claim a spin-transition at the nanometric regime.

Later, Bousseksou produced 3-D coordination polymers derived from $[Fe^{II}(azpy)(M^{II}(CN)_4)]\cdot nH_2O$ (azpy = 4,4′-azopyridine; M = Ni, Pd, and Pt), to fabricate nanopatterned thin films on gold substrates. Micro- and nanometric patterns were obtained using a PMMA mask as a physical barrier for the assembly of the multilayers on the substrate, Fig. 14.14a, b and c.[79] The authors have characterised the SCO characteristic of both bulk materials and nanopatterned materials by Raman and concluded that nanopatterned thin films on gold substrates retained their SCO characteristics, Fig. 14.14d and e.

Recently, Bousseksou and Salmon used the previously described methods to fabricate micro- and nanopatterned thin layers of the compound [Fe(bpac)($M(CN)_4$)] (bpac = bis(4-pyridyl)acetylene; M = Ni, Pd, and Pt) with pattern sizes of 2000, 200 and 30 nm.[80] The authors investigated the uptake of guest solvent molecules by the porous patterns and observed that the SCO behaviour is different and reversible when inclusion of pyridine occurred.

Finally, Vieu *et al.* reported their work on soft lithographic patterning of SCO nanoparticles using micro-transfer moulding (μTM) to pattern [Fe(NH_2trz)](tos)$_2$ (tos = tosylate, NH_2trz = 4-amino-1,2,4-triazole). This SCO compound is known to exhibit a relatively abrupt thermal transition between the HS and LS forms around room temperature. To form such patterns of SCO nanoparticles, a drop of the nanoparticle suspension was placed on the patterned surface of a PDMS stamp and the excess solution was removed by a stream of nitrogen until the PDMS stamp was completely dry. Finally, the filled stamp was placed in contact with a substrate and peeled away.[81] Using this method the authors fabricated micrometric features of 5 μm meshes that were perfectly ordered with no defects. The resolution limit of the patterned stripes was further moved into the nanometer regime by using μTM. Structures with a resolution of approximately 300 nm could be achieved with good thickness homogeneity and very few defects. Despite the difficulties in assigning the SCO transition of the patterned nanoparticles because the spectrum of the microstructures is dominated by the strong Raman scattering of the NaAOT surfactant used during the fabrication process of the nanoparticles, the authors claimed to have prepared micro- and nanopatterns of SCO nanoparticles retaining their spin switching characteristic after fabrication of such materials.

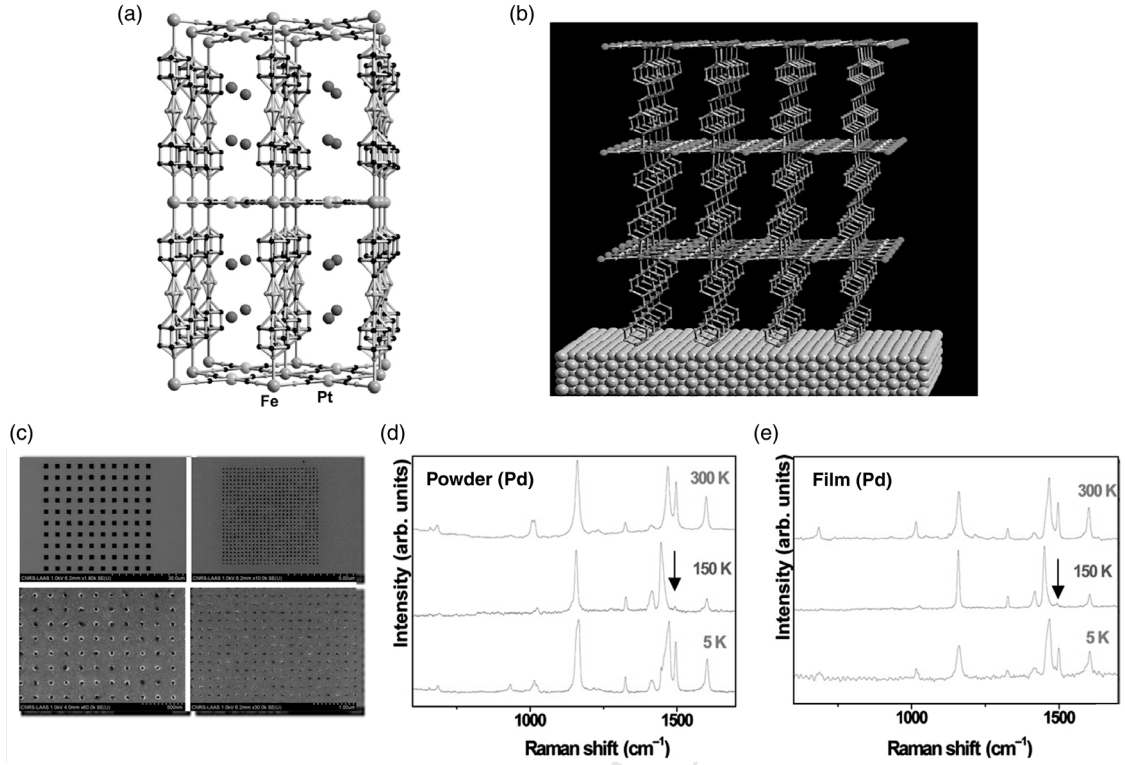

Figure 14.14 *Templating of SCO nanostructures: (a) 3-D coordination polymer of $[Fe^{II}(azpy)(M^{II}(CN)_4)]\cdot nH_2O$; (b) scheme of deposition of 3-D coordination polymer on gold surface; (c) SEM images of patterns of $Fe(azpy)[Pd(CN)_4]$ obtained following 10 deposition cycles for different shapes with distinct sizes between 2 μm and 30 nm; (d) variable temperature Raman spectra of bulk material indicating SCO; (e) variable temperature Raman spectra of nanopatterns indicating SCO. Reproduced from ref. 79. Copyright American Chemical Society.*

14.5 Electrical Spin State Control

Fabrication of typical data storage devices is performed using a *top-down* approach where the size of discrete magnetic domains is constantly reduced in dimensions.[82] The size of discrete magnetic domains can be reduced until the super paramagnetic limit is reached, where ambient temperature is sufficient to invert the magnetisation of such domains leading to highly unstable devices.[83, 84] To overcome this problem scientists have been developing strategies using diverse and imaginative solutions such as antiferromagnetic coupling media recording,[85] perpendicular recording[86] and lithographically patterned media recording,[87] while the assembly of magnetic molecules into nanowires has been reported producing a huge advance in the area of information storage.[88, 89]

In a complementary *bottom-up* approach, chemists have applied supramolecular principles to fabricate molecular machines, motors and switches, and devices for information storage and processing represent a particularly attractive field in this research area. For example, reversible data storage may become possible on the nanoscale by imprinting information via a change of magnetisation. Reversibility of this process requires materials with variable magnetisation states that can be addressed selectively and without perturbation of

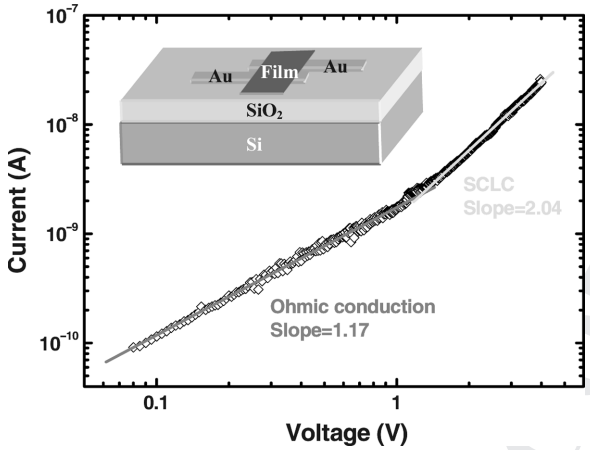

Figure 14.15 *Electrical properties of a SCO film: current–voltage characteristics for a 240 nm thick film of [Fe(phen)$_2$(SCN)$_2$] evaporated on a silicon substrate at 300 K and linear fits to the data. Reproduced from ref. 72. Copyright American Institute of Physics.*

the entire environment. Research has been developed where bistable magnetic states are addressed mainly by application of temperature or light. For electronic purposes, it is desirable to apply an electric field to switch between two states which would permit fabrication of molecular devices where the magnetic states are controlled electrically.

Studies on attempts to electrically control the spin states on SCO complexes are quite recent and the first studies on devices have been reported by Shi and Beaurepaire, Fig. 14.15.[72] A device was constructed using a 240 nm thick film of [Fe(phen)$_2$(SCN)$_2$] evaporated on a silicon substrate with gold electrodes. The current–voltage (*I*-*V*) characteristics at room temperature of the device were determined, and at low voltage the ln(*I*)-ln(*V*) characteristic is linear with a slope of 1.17 suggesting Ohmic conduction. Above 1.4 V, the ln(*I*)-ln(*V*) characteristic remained linear but with a slope of 2.04, indicating a space charge-limited current (SCLC) regime. The authors extracted a mobility of 6.53×10^{-6} cm^2/Vs in the space charge-limited regime, comparable to that found in typical small organic molecules.

Developments of Coronado's work with SCO nanoparticles reported in 2007 have been recently achieved, where Coronado and van der Zant described devices built from a single SCO nanoparticle.[90] Nanoparticles based on a core of the Fe(II) coordination polymer [Fe(trz)$_3$](BF$_4$)$_2$ (trz = triazole) and a surfactant shell around 11 nm in diameter were placed between two nanometer-spaced electrodes. Such particles have been characterised in detail and show a cooperative spin-transition from Fe(II) low spin, $S = 0$, to high spin, $S = 2$, exhibiting a thermal hysteresis loop above room temperature with a width of ca. 40 K.[21, 24]

Current–voltage (*I*–*V*) experiments at 10 K led to the observation that for the 100-nm-wide electrode, equidistant step-like features and peaks in the corresponding derivative

(d*I*/d*V*), are reminiscent of a Coulomb staircase. Based on these observations, the authors concluded that the transport mechanism is due to sequential single-electron tunnelling through an asymmetric double-barrier junction. The nanoparticle core is isolated from the electrodes by tunnel barriers defined by the surfactant layer where, electrons first tunnel onto the particle and remain there for some time before tunnelling off again. Coulomb steps are equidistant and therefore indicate that transport occurs through a single particle.

The current–voltage characteristics of the devices measured between 300–400 K show that there was a change in conductance in the temperature region of the SCO. Moreover, a hysteresis loop was observed in the current–voltage characteristic of the devices, although this was only observed in 30% of the devices

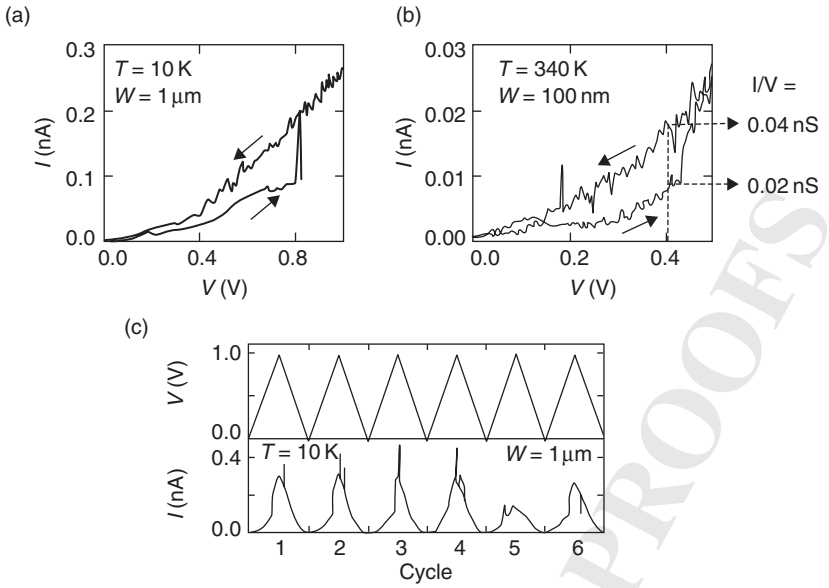

Figure 14.16 *Device of $[Fe(trz)_3](BF_4)_2$SCO nanoparticles: (a) Current–voltage characteristics of a 1-μm-wide electrode device at low temperature; (b) current–voltage characteristic of a 100-nm-wide electrode device at 340 K. The conductance (I/V) at 0.4 V coincides with the values observed in the thermal hysteresis of the same device, showing that the bistability can be probed with an applied voltage; (c) repetitive cycling of the voltage between 0 and 1 V at low temperature (10 K) of the device. Reproduced from ref. 90. Copyright Wiley/VCH.*

tested. The authors found that by keeping the temperature constant but changing the applied bias voltage, a transition between the low- and the high-conductance state occurs, being the effect more pronounced at low temperature, Fig. 14.16.

The device whose conductance is represented in Fig. 14.16a was cycled 6 times and it was observed that the lifetime of the high-conductance states varies. Factors such as electric field polarisation, intersystem crossing through excited states and local resistive heating are possible explanations for this observation.

More recently, Ruben and van der Zant reported on the electrical control of SCO in a single molecule.[91] The approach used by the authors was different from that previously reported, where SCO is triggered by charging the molecule with two electrons. This was predicted by theoretical calculations and confirmed experimentally by a split of zero bias (Kondo) resonance in the current–voltage characteristics. Theoretical calculations suggest that the spin-transition should manifest itself in an electron transport experiment by the specific structure of its magnetic excitations and experiments were carried out with a three terminal device and the low-energy excitation probed by inelastic tunnelling spectroscopy. Transport experiments revealed a double-quantum-dot behaviour in combination with a split Kondo peak, Fig. 14.17. This experiment opens the realm of active spin state modulation in a molecule; the smallest possible SCO switching unit.

Finally, Bousseksou reports on electrical properties and the nonvolatile memory effect of a SCO complex.[92] The authors built a nonvolatile memory device based on changes of the dielectric permittivity allowing the information to be stored in the high- and low-capacitance states. The compound elected for these studies was $[Fe(HB(pz)_3)_2]$ where $HB(pz)_3$ = hydrotris(1-pyrazolyl)borate. This compound is known to undergo a thermal spin transition in the 300–450 K temperature range with the first heating cycle completely different from successive thermal cycles. Such a difference has been attributed to a crystallographic transformation.

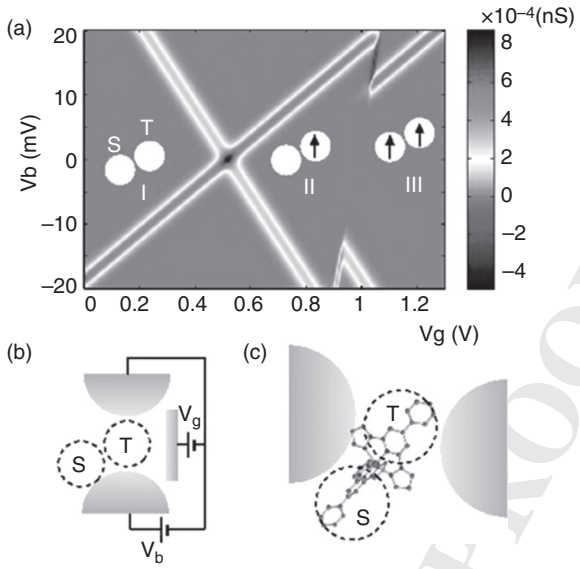

Figure 14.17 *(a) Simulation of the differential conductance vs. source-drain (V_b) and gate (Vg) voltages calculated for T = 4.2 K; (b) schematic representation of the double-dot system. T: transfer dot, S: spectator dot; (c) schematic representation of molecule-electrode contacts realising the double-dot system. Reproduced from ref. 91. Copyright American Physical Society.*

Thin films of the compound, of ca. 200 nm thickness, were deposited on gold interdigitated microelectrodes by thermal evaporation and the composition of the films was confirmed by Raman spectroscopy.

The resulting thin film had a densely covered surface with a granular morphology composed of nanocrystals, and was used for AC conductivity measurements as a function of frequency and temperature. Isothermal frequency measurements revealed a change in conductivity with a frequency dependence more pronounced than in the powdered sample, which the authors attributed to a higher degree of disorder of the thin films. I-V measurements were performed on a thin film, at room temperature, before and after heating the film to 408 K, showing that these differ considerably. A complementary experiment was carried out by changing the applied electric bias from 1 to 10 V. An increase in current was observed upon changing the applied bias from 1 to 2 V, but over time the current drops to low conductivity values. A further increase in voltage showed a small increase in current, which remained in the low conductivity region. Based on these observations the authors claimed the construction of a nonvolatile read-only memory (ROM) using a SCO compound.

14.6 Conclusion

SCO is a fascinating interdisciplinary area of research which has attracted experimentalists and theoreticians from chemistry, physics, materials science and engineering. SCO research emerged 80 years ago and a long and impressive literature on SCO has been developed with the discovery of several new examples of SCO compounds, the explanation of different types of SCO profiles and the modification of SCO examples to increase cooperativity and to direct the application to materials science. The development of materials from SCO molecules has attracted scientists and has been a very active area in recent years. These include the fabrication of SCO nanoparticles and nanocrystals, the fabrication of SCO thin films, the use of patterning

techniques to fabricate SCO nanostructures and more recently the fabrication of devices using SCO materials where spin states are addressed electrically.

SCO nanoparticles are of great interest and have shown to display interesting properties. Reports on SCO nanoparticles and nanocrystals are limited to a few research groups and it will be important in the future to investigate physical properties of a single particle and size effects on physical properties. Also, new examples of nanoparticles and other nano-objects with higher control of size and spatial orientation of the SCO molecules in the nano-objects would be desirable.

Fabrication of SCO thin films was a very active area in former years with work initiated by Kahn and built on by others. Unfortunately, due to the lack of predictability and control this area has been neglected. Undoubtedly, the most interesting method for producing regular thin films is the ultra-high vacuum deposition of thin films. This lacks examples due to the limitation of the method to molecules that are stable under the deposition conditions. New examples of neutral SCO molecules would help to advance this field.

Patterning of SCO molecules permits the fabrication of materials with different sizes and shapes which is very appealing for materials development and device fabrication. The major drawback of this technique is its cost and processing times, and without new cost-effective hardware to produce nanopatterned materials, this will not be pushed forward.

Finally, devices where spin states are addressed electrically, in particular at the single molecule limit, are the most interesting and important of the advances in SCO research towards application of SCO materials. This would permit the fabrication of cost-effective hybrid assemblies, where SCO molecules or objects are integrated into electronic circuits acting as active switching units in spintronic devices.[93]

References

1. Cambi, L., Szegö, L. (1931) Über die magnetische Susceptibilität der komplexen Verbindungen. Ber. Dtsch. Chem. Ges. Teil B, 64: 2591–2598.
2. Kahn, O., Codjovi, E., Garcia, Y., van Koningsbruggen, P. J., Lapouyade, R., Sommier, L. (1996) Spin-transition molecular materials for display and data processing. ACS Symp. Ser., 644: 298–310.
3. Erenburg, S. B., Bausk, N. V., Lavrenova, L. G., Varnek, V. A., Mazalov, L. N. (1997) Relation between electronic and spatial structure and spin-transition parameters in chain-like Fe(II) compounds. Solid State Ionics, 101: 571–577.
4. Garcia, Y., van Koningsbruggen, P. J., Lapouyade, R., Fournès, L., Rabardel, L., Kahn, O., Ksenofontov, V., Levchenko, G., Gütlich, P. (1998) Influences of temperature, pressure, and lattice solvents on the spin transition regime of the polymeric compound $[Fe(hyetrz)_3]A_2{\cdot}3H_2O$ (hyetrz = 4-(2′-hydroxyethyl)-1,2,4-triazole and A^- = 3-nitrophenylsulfonate). Chem Mater, 10: 2426–2433.
5. Garcia, Y., Niel, V., Muñoz, M. C., Real, J. A.(2004) Spin crossover in 1D, 2D and 3D polymeric Fe(II) networks, in: Gütlich, P., Goodwin, H. A. (Eds) Spin Crossover in Transition Metal Compounds I. Top. Curr. Chem., 233: 229–257.
6. Ruben, M., Ziener, U., Lehn, J.-M., Ksenofontov, V., Gütlich, P., Vaughan, G. B. M. (2004) Hierarchical self-assembly of supramolecular spintronic modules into 1D- and 2D-architectures with emergence of magnetic properties. Chem. Eur. J., 11: 94–100.
7. Kitazawa, T., Gomi, Y., Takahashi, M., Takeda, M., Enomoto, M., Miyazaki, A,. Enoki, T. (1996) Spin-crossover behaviour of the coordination polymer $Fe^{II}(C_5H_5N)_2Ni^{II}(CN)_4$. J. Mater. Chem., 6: 119–121.
8. Niel, V., Martinez-Agudo, J.M., Muñoz, M. C., Gaspar, A. B., Real, J. A. (2001) Cooperative spin crossover behavior in cyanide-bridged Fe(II)-M(II) bimetallic 3D Hofmann-like networks (M = Ni, Pd, and Pt). Inorg. Chem., 40: 3838–3839.
9. Roubeau, O., Colin, A., Schmitt, W., Clérac, R. (2004) Thermoreversible gels as magneto-optical switches. Angew. Chem. Int. Ed., 43: 3283–3286.

10. Grondin, P., Roubeau, O., Castro, M., Saadaoui, H., Colin, A., Clérac, R. (2010) Multifunctional gels from polymeric spin-crossover metallo-gelators. Langmuir, 26: 5184–5195.
11. Fujigaya, T., Jiang, D. L., Aida, T. (2007) Spin-crossover physical gels: a quick thermoreversible response assisted by dynamic self-organization. Chem. Asian J., 2:106–113.
12. Galyametdinov, Y., Ksenofontov, V., Prosvirin, A., Ovchinnikov, I., Ivanova, G., Gütlich, P., Haase, W. (2001) First example of coexistence of thermal spin transition and liquid-crystal properties. Angew. Chem. Int. Ed., 40: 4269–4271.
13. Bodenthin, Y., Schwarz, G., Tomkowicz, Z., Lommel, M., Geue, T., Haase, W., Mohwald, H., Pietsch, U., Kurth, D. G. (2009) Spin-crossover phenomena in extended multi-component metallo-supramolecular assemblies. Coord. Chem. Rev., 253: 2414–2422.
14. Gaspar, A.B., Seredyuk, M., Gütlich, P. (2009) Spin crossover in metallomesogens. Coord. Chem. Rev., 253: 2399–2413.
15. Gütlich, P., Goodwin, H. A. (2004) Spin crossover–an overall perspective, in: Gütlich, P., Goodwin, H. A. (Eds) Spin Crossover in Transition Metal Compounds I. Top. Curr. Chem., 233: 1–47.
16. Cambi, L., Szegö, L. (1933) Über die magnetische Susceptibilität der komplexen Verbindungen (II. Mitteil.). Ber. Dtsch. Chem. Ges. Teil B, 66 (1933) 656–661.
17. Cambi, L., Malatesta, L. (1937) Magnetismus und Polymorphie innerer Komplexsalze: Eisensalze der Dithiocarbamidsäuren. Ber. Dtsch. Chem. Ges. Teil B, 70: 2067–2078.
18. Létard, J.-F., Guionneau, P., Goux-Capes, L. (2004) Towards spin crossover applications, in: Gütlich, P., Goodwin, H. A. (Eds) Spin Crossover in Transition Metal Compounds III. Top. Curr. Chem., 235: 221–249.
19. Catala, L., Volatron, F., Brinzei, D., Mallah, T. (2009) Functional coordination nanoparticles. Inorg. Chem., 48: 3360–3370.
20. Neville, S. M., Etrillard, C., Asthana, S., Létard, J.-F. (2010) Light-induced stored information in nanoparticles. Eur. J. Inorg. Chem., 282–288.
21. Coronado, E., Galán-Mascarós, J. R., Monrabal-Capilla, M., García-Martínez, J., Pardo-Ibáñez, P. (2007) Bistable spin-crossover nanoparticles showing magnetic thermal hysteresis near room temperature. Adv. Mater., 19: 1359–1362.
22. Forestier, T., Mornet, S., Daro, N., Nishihara, T., Mouri, S., Tanaka, K., Fouché, O., Freysz, E., Létard, J.-F. (2008) Nanoparticles of iron(II) spin-crossover. Chem. Commun., 36: 4327–4329.
23. Forestier, T., Kaiba, A., Pechev, S., Denux, D., Guionneau, P., Etrillard, C., Daro, N., reysz, E., Létard, J.-F. (2009) Nanoparticles of $[Fe(NH_2\text{-trz})_3]Br_2{\cdot}3H_2O$ (NH_2-trz = 2-amino-1,2,4-triazole) prepared by the reverse micelle technique: influence of particle and coherent domain sizes on spin-crossover properties. Chem. Eur. J., 15: 6122–6130.
24. Galán-Mascarós, J.R., Coronado, E., Forment-Aliaga, A., Monrabal-Capilla, M., Pinilla-Cienfuegos, E., Ceolin, M. (2010) Tuning size and thermal hysteresis in bistable spin crossover nanoparticles. Inorg. Chem., 49: 5706–5714.
25. Salmon, L., Molnár, G., Zitouni, D., Quintero, C., Bergaud, C., Micheau, J.-C., Bousseksou, A. (2010) A novel approach for fluorescent thermometry and thermal imaging purposes using spin crossover nanoparticles. J. Mater. Chem., 20: 5499–5503.
26. Dutt, G. B. (2008) Fluorescence anisotropy of ionic probes in AOT reverse micelles: influence of water droplet size and electrostatic interactions on probe dynamics. J. Phys. Chem. B, 112: 7220–7226.
27. Tokarev, A., Salmon, L., Guari, Y., Nicolazzi, W., Molnár, G., Bousseksou, A. (2010) Cooperative spin crossover phenomena in $[Fe(NH_2trz)_3](tosylate)_2$ nanoparticles. Chem. Commun., 46: 8011–8013.
28. Titos-Padilla, S., Herrera, J. M., Chen, X.-W., Delgado, J. J., Colacio, E. (2011) Bifunctional hybrid SiO_2 nanoparticles showing synergy between core spin crossover and shell luminescence properties. Angew. Chem. Int. Ed., 50: 3290–3293.
29. Kröber, J., Audière, J.-P., Claude, R., Codjovi, E., Kahn, O., Haasnoot, J. G., Grolière, F., Jay, C., Bousseksou, A. (1994) Spin transitions and thermal hystereses in the molecular – based materials $[Fe(Htrz)_2(trz)](BF_4)$ and $[Fe(Htrz)_3](BF_4)_2{\cdot}H_2O$ (Htrz = 1,2,4-4*H*-triazole; trz = 1,2,4- triazolato) Chem. Mater., 6: 1404–1412.
30. Mader, D., Pillet, S., Carteret, C., Stébé, M.-J., Blin, J.-L. (2011) Confined growth of spin crossover nanoparticles in surfactant-based matrices: enhancing shape anisotropy. J. Dispers. Sci. Tech., 32: 1771–1779.
31. Volatron, F., Catala, L., Rivière, E., Gloter, A., Stéphan, O., Mallah, T. (2008) Spin-crossover coordination nanoparticles. Inorg. Chem., 47: 6584–6586.

32. Raza, Y., Volatron, F., Moldovan, S., Ersen, O., Huc, V., Martini, C., Brisset, F., Gloter, A., Stéphan, O., Bousseksou, A., Catala, L., Mallah, T. (2011) Matrix-dependent cooperativity in spin crossover Fe(pyrazine)$Pt(CN)_4$ nanoparticles. Chem Commun, 47: 11501–11503.
33. Martínez, V., Boldog, I., Gaspar, A. B., Ksenofontov, V., Bhattacharjee, A., Gütlich, P., Real, J. A. (2010) Spin crossover phenomenon in nanocrystals and nanoparticles of $[Fe(3\text{-}Fpy)_2M(CN)_4]$ (M^{II} = Ni, Pd, Pt) two-dimensional coordination polymers. Chem. Mater., 22: 4271–4281.
34. Boldog, I., Gaspar, A. B., Martínez, V., Pardo-Ibañez, P., Ksenofontov, V., Bhattacharjee, A., Gütlich, P., Real, J. A. (2008) Spin-crossover nanocrystals with magnetic, optical, and structural bistability near room temperature. Angew. Chem. Int. Ed., 47: 6433–6437.
35. Larionova, J., Salmon, L., Guarl, Y., Tokarev, A., Molvinger, K., Molnár, G., Bousseksou, A. (2008) Towards the ultimate size limit of the memory effect in spin-crossover solids. Angew. Chem. Int. Ed., 47: 8236–8240.
36. Tissot, A., Bardeau, J.-F., Rivière, E., Brisset, F., Boillot, M.-L. (2010) Thermo- and photoswitchable spin-crossover nanoparticles of an iron(II) complex trapped in transparent silica thin films. Dalton Trans., 39: 7806–7812.
37. Faulmann, C., Chahine, J., Malfant, I., de Caro, D., Cormary, B., Valade, L. (2011) A facile route for the preparation of nanoparticles of the spin-crossover complex $[Fe(Htrz)_2(trz)](BF_4)$ in xerogel transparent composite films. Dalton Trans., 40: 2480–2485.
38. Talham, D. R. (2004) Conducting and magnetic Langmuir−Blodgett films. Chem. Rev., 104: 5479–5502.
39. Ruaudel-Teixier, A., Barraud, A., Coronel, P., Kahn, O. (1988) Spin transition in a magnetic Langmuir-Blodgett film. Thin Solid Films, 160: 107–115.
40. Coronel, P., Barraud, A., Claude, R., Kahn, O., Ruaudel-Teixier, A., Zarembowitch, J. (1989) Spin transition in a Langmuir–Blodgett film. J. Chem. Soc. Chem. Commun., 3: 193–194.
41. Soyer, H., Mingotaud, C., Boillot, M.-L., Delhaès, P. (1998) Spin-crossover complex stabilized on a formamide/water subphase. Thin Solid Films, 329: 435–438.
42. Soyer, H., Mingotaud, C., Boillot, M.-L., Delhaès, P. (1998) Spin crossover of a Langmuir-Blodgett film based on an amphiphilic iron(II) complex. Langmuir, 14: 5890–5895.
43. Soyer, H., Dupart, E., Gómez-García, C. J., Mingotaud, C., Delhaès, P. (1999) First magnetic observation of a spin crossover in a Langmuir-Blodgett film. Adv. Mater., 11: 382–384.
44. Létard, J.-F., Nguyen, O., Soyer, H., Mingotaud, C., Delhaès, P., Kahn, O. (1999) First evidence of the LIESST effect in a Langmuir-Blodgett film. Inorg. Chem., 38: 3020–3021.
45. Soyer, H., Dupart, E., Mingotaud, C., Gomez-Garcia, C. J., Delhaès, P. (2000) Spin crossover phenomenon of a semi-fluorinated iron (II) complex organized in a Langmuir-Blodgett film. Colloids Surf. A, 171: 275–282.
46. Armand, F., Badoux, C., Bonville, P., Ruaudel-Teixier, A., Kahn, O. (1995) Langmuir-Blodgett films of spin transition iron(II) metalloorganic polymers. 1. Iron(II) complexes of octadecyl-1,2,4-triazole. Langmuir, 11: 3467–3472.
47. Roubeau, O., Agricole, B., Clérac, R., Ravaine, S. (2004) Triazole-based magnetic Langmuir−Blodgett films: paramagnetic to spin-crossover behavior. J. Phys. Chem. B, 108: 15110–15116.
48. Roubeau, O., Natividad, E., Agricole, B., Ravaine, S. (2007) Formation, structure, and morphology of triazole-based Langmuir−Blodgett films. Langmuir, 23: 3110–3117.
49. Kurth, D. G., Lehmann, P., Schütte, M. (2000) A route to hierarchical materials based on complexes of metallo-supramolecular polyelectrolytes and amphiphiles. Proc. Natl. Acad. Sci. USA, 97: 5704–5707.
50. Lehmann, P., Kurth, D. G., Brezesinski, G., Symietz, C. (2001) Structural analysis of a metallosupramolecular polyelectrolyte-amphiphile complex at the air/water interface. Chem. Eur. J., 7: 1646–1651.
51. Bodenthin, Y., Pietsch, U., Möhwald, H., Kurth, D. G. (2005) Inducing spin crossover in metallo-supramolecular polyelectrolytes through an amphiphilic phase transition. J. Am. Chem. Soc., 12: 3110–3114.
52. Bodenthin, Y., Schwarz, G., Tomkowicz, Z., Nefedov, A., Lommel, M., Möhwald, H., Haase, W., Kurth, D. G., Pietsch, U. (2007) Structure-driven remanent high-spin state in metallosupramolecular assemblies. Phys. Rev. B, 76: 64422/1–064422/6.
53. White, N. G., Feltham, H. L. C., Gandolfi, C., Albrecht, M., Brooker, S. (2010) Towards Langmuir–Blodgett films of magnetically interesting materials: solution equilibria in amphiphilic iron(II) complexes of a triazole-containing ligand. Dalton Trans., 39: 3751–3758.

54. Kitchen, J. A., White, N. G., Gandolfi, C., Albrecht, M., Jameson, G. N. L., Tallon, J. L., Brooker, S. (2010) Room-temperature spin crossover and Langmuir–Blodgett film formation of an iron(II) triazole complex featuring a long alkyl chain substituent: the tail that wags the dog. Chem. Commun., 46: 6464–6466.
55. Gandolfi, C., Miyashita, N., Kurth, D. G., Martinho, P. N., Morgan, G. G., Albrecht, M. (2010) Organization of spin- and redox-labile metal centers into Langmuir and Langmuir–Blodgett films. Dalton Trans., 39: 4508–4516.
56. Gandolfi, C., Moitzi, C., Schurtenberger, P., Morgan, G. G., Albrecht, M. (2008) Improved cooperativity of spin-labile iron(III) centers by self-assembly in solution. J. Am. Chem. Soc., 130: 14434–14435.
57. Morgan, G. G., Murnaghan, K. D., Müller-Bunz, H., Mckee, V., Harding, C. J. (2006) A manganese(III) complex that exhibits spin crossover triggered by geometric tuning. Angew. Chem. Int. Ed., 45: 7192–7195.
58. Bell, C. M., Keller, S. W., Lynch, V. M., Mallouk, T. E. (1993) New solids and surfaces, via coordination chemistry. Mater. Chem. Phys., 35: 225–232.
59. Bell, C. M., Arendt, M. F., Gomez, L., Schmehl, R. H., Mallouk, T. E. (1994) Growth of lamellar Hofmann clathrate films by sequential ligand exchange reactions: assembling a coordination solid one layer at a time. J. Am. Chem. Soc., 116: 8374–8375.
60. Cobo, S., Molnár, G., Real, J. A., Bousseksou, A. (2006) Multilayer sequential assembly of thin films that display room-temperature spin crossover with hysteresis. Angew. Chem. Int. Ed., 45: 5786–5789.
61. Wang, Y., Zhou, W. (2010) A review on inorganic nanostructure self-assembly. J. Nanosci. Nanotech., 10: 1563–1583.
62. Matsuda, M., Tajima, H. (2007) Thin film of a spin crossover complex $[Fe(dpp)_2](BF_4)_2$. Chem. Lett., 36: 700–701.
63. Matsuda, M., Isozaki, H., Tajima, H. (2008) Electroluminescence quenching caused by a spin-crossover transition. Chem Lett, 37: 374–375.
64. Liu, X. J., Moritomo, Y., Nakamura, A., Hirao, T., Toyazaki, S., Kojima, N. (2001) Photoinduced phase transition and relaxation behavior in a spin-crossover Fe(II) complex Nafion-$[Fe(Htrz)_3]$ film. J. Phys. Soc. Jpn., 70: 2521–2524.
65. Kojima, N., Toyazaki, S., Itoi, M., Ono, Y., Aoki, W., Kobayashi, Y., Seto, M., Yokoyama, T. (2002) Search on multi-functional properties of spin-crossover system. Mol. Cryst. Liq. Cryst., 376: 567–574.
66. Nakamoto, A., Ono, Y., Kojima, N., Matsumura, D., Yokoyama, T., Liu, X. J., Moritomo, Y. (2003) Spin transition and its photo-induced effect in spin crossover complex film based on $[Fe(II)(trz)_3]$. Synth. Met., 137:1219–1220.
67. Liu, X. J., Moritomo, Y., Kawamoto, T., Nakamoto, A., Kojima, N. (2003) Dynamical phase transition in a spin-crossover complex. J. Phys. Soc. Jpn., 72: 1615–1618.
68. Nakamoto, A., Ono, Y., Kojima, N., Matsumura, D., Yokoyama, T. (2003) Spin crossover complex film, $[Fe^{II}(H\text{-}trz)_3]$-Nafion, with a spin transition around room temperature. Chem. Lett., 32: 336–337.
69. Nakamoto, A., Kojima, N., Liu, X. J., Moritomo, Y., Nakamura, A. (2005) Demonstration of the thermally induced high spin–low spin transition for a transparent spin crossover complex film $[Fe(II)(H\text{-}trz)_3]$-Nafion (trz = triazole). Polyhedron, 24: 2909–2912.
70. Kamebuchi, H., Jo, T., Shimizu, H., Okazawa, A., Enomoto, M., Kojima, N. (2011) Development of pH-sensitive spin-crossover iron(II) complex films, $[Fe^{II}(diAMsar)]$-Nafion: manipulation of the spin state by proton concentration. Chem. Lett., 40: 888–889.
71. Boillot, M.-L., Pillet, S., Tissot, A., Rivière, E., Claiser, N., Lecomte, C. (2009) Ligand-driven light-induced spin change activity and bidirectional photomagnetism of styrylpyridine iron(II) complexes in polymeric media. Inorg. Chem., 48: 4729–4736.
72. Shi, S., Schmerber, G., Arabski, J., Beaufrand, J. B., Kim, D. J., Boukari, S., Bowen, M., Kemp, N. T., Viart, N., Rogez, G., Beaurepaire, E., Aubriet, H., Petersen, J., Becker, C., Ruch, D. (2009) Study of molecular spin-crossover complex $Fe(phen)_2(NCS)_2$ thin films. Appl. Phys. Lett., 95: 043303/1–043303/3.
73. Naggert, H., Bannwarth, A., Chemnitz, S., von Hofe, T., Quandt, E., Tuczek, F. (2011) First observation of light-induced spin change in vacuum deposited thin films of iron spin crossover complexes. Dalton Trans., 40: 6364–6366.
74. Moliner, N., Salmon, L., Capes, L., Muñoz, M. C., Létard, J.-F., Bousseksou, A., Tuchagues, J.-P., McGarvey, J. J., Dennis, A. C., Castro, M., Burriel, R., Real, J. A. (2002) Thermal and optical switching of molecular spin states in the $\{[FeL[H_2B(pz)_2]_2\}$ spin-crossover system (L = bpy, phen). J. Phys. Chem. B, 106: 4276–4283.
75. Cavallini, M., Bergenti, I., Milita, S., Ruani, G., Salitros, I., Qu, Z. R., Chandrasekar, R., Ruben, M. (2008) Micro- and nanopatterning of spin-transition compounds into logical structures. Angew. Chem. Int. Ed., 47: 8596–8600.
76. Baker, W. A. jr., Bobonich, H. M. (1964) Magnetic properties of some high-spin complexes of iron(II). Inorg. Chem., 3: 1184–1188.

77. Cavallini, M., Bergenti, I., Milita, S., Kengne, J. C., Gentili, D., Ruani, G., Salitros, I., Meded, V., Ruben, M. (2011) Thin deposits and patterning of room-temperature-switchable one-dimensional spin-crossover compounds. Langmuir, 27: 4076–4081.
78. Molnár, G., Cobo, S., Real, J. A., Carcenac, F., Daran, E., Vieu, C., Bousseksou, A. (2007) A combined top-down/bottom-up approach for the nanoscale patterning of spin-crossover coordination polymers. Adv. Mater., 19: 2163–2167.
79. Agustí, G., Cobo, S., Gaspar, A. B., Molnár, G., Moussa, N.O., Szilágyi, P. A., Pálfi, V., Vieu, C., Muñoz, M. C., Real, J. A., Bousseksou, A. (2008) Thermal and light-induced spin crossover phenomena in new 3D Hofmann-like microporous metalorganic frameworks produced as bulk materials and nanopatterned thin films. Chem. Mater., 20: 6721–6732.
80. Bartual-Murgui, C., Akou, A., Salmon, L., Molnár, G., Thibault, C., Real, J. A., Bousseksou, A. (2011) Guest effect on nanopatterned spin-crossover thin films. Small, 7: 3385–3391.
81. Thibault, C., Molnár, G., Salmon, L., Bousseksou, A., Vieu, C. (2010) Soft lithographic patterning of spin crossover nanoparticles. Langmuir, 26: 1557–1560.
82. Dietzel, A. (2003) Hard disk drives, in: Waser, R. (Ed.) Nanoelectronics and Information Technology. Wiley-VCH, Berlin, p. 617–631.
83. Charap, S. H., Lu, P. L., He, Y. J. (1997) Thermal stability of recorded information at high densities. IEEE Trans. Magn., 33: 978–983.
84. Martín, J. I., Nogués, J., Liu, K., Vicent, J. L., Schuller, I. K. (2003) Ordered magnetic nanostructures: fabrication and properties. J. Magn. Magn. Mater., 256: 449–501.
85. Skumryev, V., Stoyanov, S., Zhang, Y., Hadjipanayis, G., Givord, D., Nogués, J. (2003) Beating the superparamagnetic limit with exchange bias. Nature, 423: 850–853.
86. Iwasaki, S., Takemura, K. (1975) An analysis for the circular mode of magnetization in short wavelength recording. IEEE Trans. Magn., 11: 1173–1175.
87. Terris, B., Thomson, T., Hu, G. (2007) Patterned media for future magnetic data storage. Microsystem Technol., 13: 189–196.
88. Thomas, L., Hayashi, M., Jiang, X., Moriya, R., Rettner, C., Parkin, S. (2007) Resonant amplification of magnetic domain-wall motion by a train of current pulses. Science, 315 (2007) 1553–1556.
89. Thomas, L., Hayashi, M., Jiang, X., Moriya, R., Rettner, C., Parkin, S. S. P. (2006) Oscillatory dependence of current-driven magnetic domain wall motion on current pulse length. Nature, 443: 197–200.
90. Prins, F., Monrabal-Capilla, M., Osorio, E. A., Coronado, E., van der Zant, H. S. J. (2011) Room-temperature electrical addressing of a bistable spin-crossover molecular system. Adv. Mater., 23: 1545–1549.
91. Meded, V., Bagrets, A., Fink, K., Chandrasekar, R., Ruben, M., Evers, F., Bernand-Mantel, A., Seldenthuis, J. S., Beukman, A., van der Zant, H. S. J. (2011) Electrical control over the Fe(II) spin crossover in a single molecule: theory and experiment. Phys. Rev. B, 8: 245415/1–245415/13.
92. Mahfoud, T., Molnár, G., Cobo, S., Salmon, L., Thibault, C., Vieu, C., Demont, P., Bousseksou, A. (2011) Electrical properties and non-volatile memory effect of the [Fe(HB(pz)3)2] spin crossover complex integrated in a microelectrode device. Appl. Phys. Lett., 99: 053307/1–053307/3.
93. Osorio, E., Bjornholm, T., Lehn, J.-M., Ruben, M., van der Zant, H. S. J. (2008) Single-molecule transport in three-terminal devices. J. Phys.: Condens. Matter, 20: 374121/1–374121/14.